European Journal of Medicinal Chemistry 247 (2023) 115033

Contents lists available at ScienceDirect

European Journal of Medicinal Chemistry

journal homepage: www.elsevier.com/locate/ejmech

Research paper

Targeted AURKA degradation: Towards new therapeutic agents for neuroblastoma

Muhammad Rishfi [a,c,1], Simon Krols [b,c,1], Fien Martens [a,c], Sarah-Lee Bekaert [a,c], Ellen Sanders [a,c], Aline Eggermont [a,c], Fanny De Vloed [a,c], Joshua Robert Goulding [a,c], Martijn Risseeuw [b,c], Jan Molenaar [d], Bram De Wilde [c,e], Serge Van Calenbergh [b,c,*], Kaat Durinck [a,c,**]

[a] Department of Biomolecular Medicine, Faculty of Medicine & Health Sciences, Ghent University, Belgium
[b] Laboratory for medicinal chemistry, Faculty of Pharmaceutical Sciences, Ghent University, Belgium
[c] Cancer Research Institute Ghent (CRIG), Ghent, Belgium
[d] Princess Máxima Center for Pediatric Oncology, Utrecht, the Netherlands
[e] Department of Internal Medicine and Pediatrics, Faculty of Medicine & Health Sciences, Ghent University, Belgium

ARTICLE INFO

Keywords:
AURKA
Neuroblastoma
PROTAC
MYCN
Targeted protein degradation

ABSTRACT

Aurora kinase A (AURKA) is a well-established target in neuroblastoma (NB) due to both its catalytic functions during mitosis and its kinase-independent functions, including stabilization of the key oncoprotein MYCN. We present a structure-activity relationship (SAR) study of MK-5108-derived PROTACs against AURKA by exploring different linker lengths and exit vectors on the thalidomide moiety. PROTAC **SK2188** induces the most potent AURKA degradation ($DC_{50,24h}$ 3.9 nM, $D_{max,24h}$ 89%) and shows an excellent binding and degradation selectivity profile. Treatment of NGP neuroblastoma cells with **SK2188** induced concomitant MYCN degradation, high replication stress/DNA damage levels and apoptosis. Moreover, **SK2188** significantly outperforms the parent inhibitor MK-5108 in a cell proliferation screen and patient-derived organoids. Furthermore, altering the attachment point of the PEG linker to the 5-position of thalidomide allowed us to identify a potent AURKA degrader with a linker as short as 2 PEG units. With this, our SAR-study provides interesting lead structures for further optimization and validation of AURKA degradation as a potential therapeutic strategy in neuroblastoma.

1. Introduction

Neuroblastoma (NB) is a childhood malignancy of the sympathetic nervous system and represents approximately 15% of all pediatric cancer deaths [1]. It arises during early embryonic development from the sympathoadrenal lineage of the neural crest. Like other embryonal tumors, NB is characterized by a low mutational burden, which limits current options for precision medicine [2]. Instead, it is driven by recurrent patterns of segmental and whole chromosomal copy-number alterations [3]. The most important example is the amplification of the *MYCN* oncogene, which is present in 20–30% of all NB tumors and is one of the strongest predictors for high-risk disease and poor overall survival [1]. Despite the clear clinical implications in NB, the development of small molecules directly targeting MYCN is challenging due to the absence of stable and well-defined binding pockets [4]. Therefore, current attempts are focused on the indirect interference with MYCN activity through pharmacological inhibition of upstream regulators (e.g., BRD4), downstream effectors (e.g., ODC1, FACT) or interacting partners that promote MYCN protein stability (e.g., PLK1 and AURKA) [5].

AURKA, AURKB and AURKC belong to the serine-threonine family of kinases. AURKA is a well-known target for therapy across several hematological and solid malignancies, including NB. Elevated AURKA expression levels are correlated to poor overall and event-free NB patient survival [6]. Functionally, AURKA is primarily known for its role in centrosome and kinetochore formation as well as mitotic spindle

* Corresponding author. Department of Biomolecular Medicine, Faculty of Medicine & Health Sciences, Ghent University, Belgium.
** Corresponding author. Department of Biomolecular Medicine, Faculty of Medicine & Health Sciences, Ghent University, Belgium.
E-mail addresses: Serge.VanCalenbergh@UGent.be (S. Van Calenbergh), Kaat.Durinck@UGent.be (K. Durinck).
[1] These authors contributed equally.

https://doi.org/10.1016/j.ejmech.2022.115033
Received 17 August 2022; Received in revised form 15 December 2022; Accepted 16 December 2022
Available online 18 December 2022

assembly during early mitosis [7]. Additionally, AURKA regulates the G2/M transition by phosphorylating PLK1 to promote mitotic entry [8], which may contribute to the proliferative advantage of malignant cells when overexpressed. Besides these well-described mitotic functions, non-canonical functions of AURKA are now becoming increasingly recognized such as MYCN protein stabilization, DNA damage repair, replication fork stabilization and its role in mediating transcription/replication conflicts by blocking MYCN-dependent transcription during S-phase [9–11]. In fact, there is a strong correlation between *AURKA* expression and *MYCN* amplification status in NB patients [6], with *AURKA* also being upregulated during TH-MYCN-driven NB formation in mice (Supplementary Fig. S1A) [12]. Although several small-molecule inhibitors exist for AURKA, these mainly inhibit its kinase-dependent mitotic functions. Certain inhibitors such as alisertib and CD532 are additionally able to displace MYCN from AURKA, but with limited efficacy [13]. In this respect, we hypothesize that AURKA protein degradation using PROteolysis TArgeting Chimeras (PROTACs) could simultaneously target both its mitotic and non-canonical functions.

PROTACS are heterobifunctional molecules that consist of three primary components: (1) a parent ligand for the protein of interest (POI), (2) an appropriate linker and (3) an E3 ubiquitin ligase-recruiting ligand. By inducing proximity between the POI and a naturally occurring E3-ligase in the form of a ternary complex, PROTACs stimulate the ubiquitination of the POI, thereby marking it for subsequent degradation by the proteasome. Currently, several PROTACs are evaluated in clinical trials [14], with ARV-471 and ARV-110 being the most clinically advanced compounds targeting the notorious estrogen and androgen receptors in breast and prostate cancer, respectively [14].

Several studies have previously described PROTACs consisting of different parent ligands capable of inducing AURKA degradation (Fig. 1) [15–17]. Alisertib-based **JB170**, for instance, was shown to induce cell cycle arrest at S-phase which is distinct from the G2/M phase observed upon treatment with alisertib [15], further indicating the kinase-independent functions of AURKA beyond mitosis. Importantly, alisertib-based PROTACs give rather incomplete degradation, which may be attributed to the centrosomal pool of AURKA being resistant to degradation, as shown for **PROTAC- D** [16]. Recently, a preprint described the discovery of PROTAC **HLB-0532259**, containing a modified version of ribociclib as AURKA ligand designed to degrade the AURKA/MYCN complex [18]. More recent efforts led to the discovery of novel PROTACs that make use of the highly selective AURKA-inhibitor MK-5108 (Fig. 2B) [19]. PROTAC **JB301** showed significantly improved degradation potency ($DC_{50,6h}$ 3 nM, $D_{max,6h}$ 82%) relative to alisertib based PROTACs in a leukemic context. Simultaneously, we investigated the use of similar MK-5108-based PROTACS in neuroblastoma and report on novel analogues with additional PEG-based linkers and a new thalidomide exit position.

2. Results

2.1. Development of AURKA-targeting PROTACs

The co-crystal structure [20] of AURKA bound to MK-5108 reveals a solvent-exposed carboxylic acid within the latter, providing a practical attachment point to synthesize candidate PROTACs (Fig. 2A). Expression data (mRNA) available through the Cancer Dependency Map repository (Broad Institute) shows that, besides leukemia, neuroblastoma displays the highest mean cereblon (CRBN) expression levels out of a total of 28 different tumor entities (Supplementary Fig. S1B). Moreover, prototypical CRBN-binders thalidomide, pomalidomide and lenalidomide are believed to result in PROTACs with superior physicochemical properties compared to those comprising other E3-ligase ligands [21, 22]. Indeed, the clinically most advanced PROTACs ARV-110 and ARV-471 also contain a CRBN ligand. Therefore, we prioritized the CRBN ligand thalidomide as E3-ligase recruiter.

It is well-established that linker lengths have a profound influence on the formation of the ternary complex, preceding ubiquitination and degradation [23–25]. Despite efforts towards rational linker design via computational approaches and structural biology, linker optimization is still a largely empirical endeavor [26–30], which led us to first explore flexible polyethylene glycol (PEG) linkers of different lengths. Besides linker lengths, their attachment sites are critical and have been reported to influence degradation potencies, selectivity and physicochemical properties [25,31–34]. Therefore, we investigate both the previously reported 4- and hitherto unexplored 5-position on the phthalimide moiety of thalidomide as linker exit vectors. An overview of the synthesized PROTACs is given in Fig. 2B.

2.2. PROTAC SK2188 efficiently degrades AURKA and destabilizes MYCN

We initially evaluated PROTACs with the linker attached on the 4-position of thalidomide in NGP cells. This cell line was chosen as a preferred *in vitro* model system because it highly expresses CRBN (Supplementary Fig. S1C), harbours a *MYCN* amplification and responds well to AURKA inhibition. Cells were treated with varying concentrations for 24h and changes in AURKA levels were monitored by Simple Western, a quantitative capillary-based Western blot assay allowing high-throughput analyses of protein lysates [35]. Fig. 3A (Supplementary Fig. S2B) shows that all PROTACS, except for **SK3250** (featuring a short 2 PEG linker), induced potent dose-dependent AURKA degradation. PROTAC **SK2188** (4 PEG units) resulted in the most potent degradation with a $DC_{50,24h}$ value of 3.9 nM and a $D_{max,24h}$ value of 89% (Fig. 3C). Replacing the ether moiety in **SK2188** and **SK2189** with an amide (**SK2186** and **SK2187**) resulted in slightly reduced degradation activity at 10 nM, but similar $D_{max,24h}$ values of 85%. Relative to

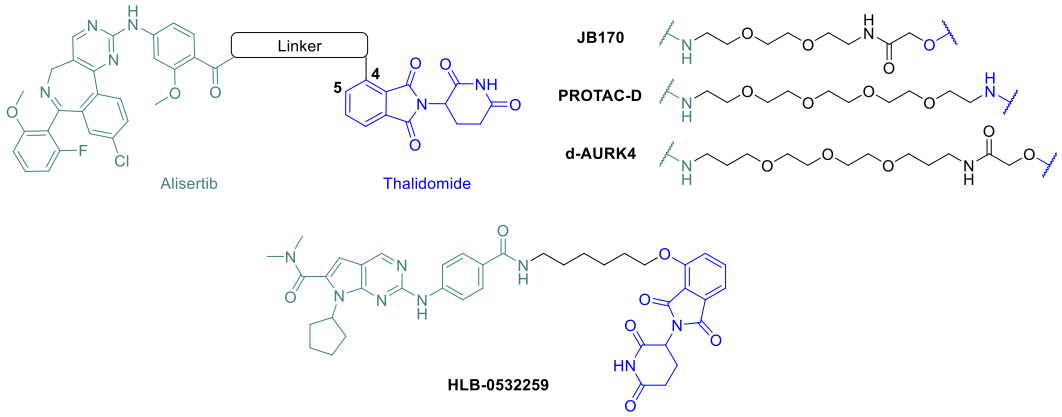

Fig. 1. Previously reported AURKA-PROTACs based on alisertib (JB170 [15], PROTAC-D [16], d-AURK4 [17]) and a ribociclib analogue (HLB-0532259) [18].

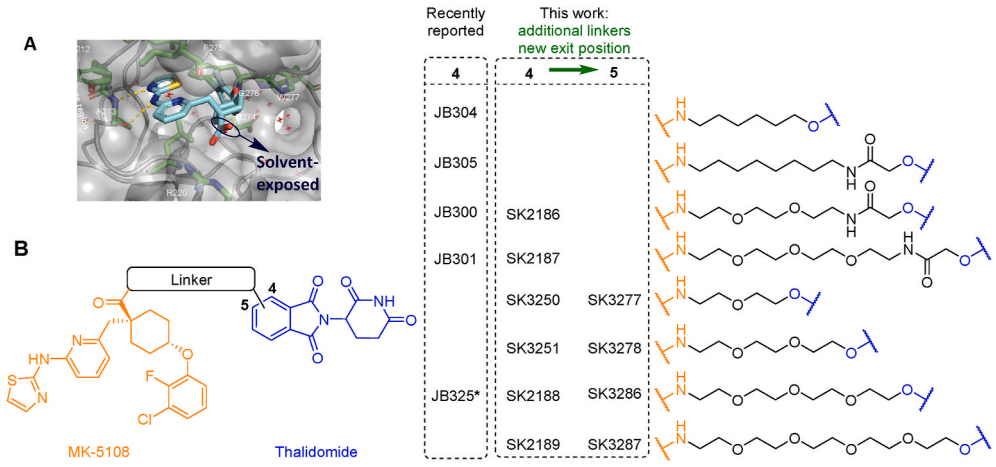

Fig. 2. (A) Co-crystal structure of AURKA (grey, key residues in green) and MK-5108 (cyan) (PDB: 5EW9). **(B)** Overview of the recently reported MK-5108-derived PROTACs [19] and PROTACs synthesized in this work. **No degradation or cell proliferation data were reported for JB325.*

MK-5108-based PROTACS, alisertib-based **JB170** displayed weaker degradation activity with a $D_{max,24h}$ value of 73%, in line with literature [15] (Fig. 3B). Consistent with previous reports, treatment with parent inhibitor MK-5108 notably resulted in a 2-fold increase of AURKA protein levels [36].

To confirm that AURKA degradation was mediated by CRBN recruitment, we synthesized and evaluated an analogue of **SK2188** (i.e., **SK3288**) containing a methylated glutarimide moiety. This analogue indeed failed to downregulate AURKA levels and, similar to inhibitor MK-5108, even led to its upregulation (Fig. 3E), confirming that CRBN binding is required for degradation. Furthermore, cells co-treated with either MK-5108 or thalidomide were successfully rescued from AURKA degradation, further confirming that binding of **SK2188** to AURKA and CRBN is required for PROTAC action (Fig. 3D). Co-treatment with proteasome inhibitor MG-132 also prevented degradation by **SK2188**, indicating that AURKA degradation is proteasome-dependent (Fig. 3F).

To evaluate AURKA degradation kinetics and assess whether this impacts MYCN protein levels, NGP cells were treated with **SK2188** at a fixed concentration and protein levels were monitored at multiple time points by western blotting (Fig. 3G & Supplementary Fig. S2D). At 500 nM, AURKA levels were reduced to 7% after 1 h and almost completely disappeared after 48h, revealing rapid and sustained degradation by **SK2188**. Interestingly, MYCN protein levels initially remain stable but are subsequently reduced starting at 24h in a time-dependent manner, with a maximum degradation of 73% at 72h. Unexpectedly, MK-5108 also resulted in MYCN depletion, albeit less efficiently than **SK2188**, with a maximum degradation of 40% at 48h, which stabilizes to 18% at 72h.

2.3. PROTAC SK2188 displays excellent AURKA binding and degradation selectivity

To assess the selectivity of **SK2188** for AURKA and exclude off-target binding effects, we first screened **SK2188** against a panel of 468 kinases via a discoverX KINOMEscan (Fig. 4A). This measures the test compounds' ability to reduce the amount of kinase captured by an immobilized ligand on a solid support and is expressed as percentage compared to control, with lower % control values corresponding to higher binding. At 1000 nM, besides AURKA (0.3% control), **SK2188** only binds 15 other kinases with a value < 35% control (standard cut-off value). Interestingly, at 100 nM only AURKA and TrkA were bound, indicating excellent target binding selectivity. As complementary approach, we also evaluated degradation selectivity by comparing short-term exposure (3h) of NGP to **SK2188** and DMSO-control through mass spectrometry-based shotgun proteome profiling (Fig. 4B). From a total of 7175 detected proteins, AURKA was the most significantly downregulated at both 100 nM ($-\log_{10} p = 11.8$, $\log_2 FC = -2.0$) and 1000 nM ($-\log_{10} p = 4.3$, $\log_2 FC = -2.0$). Cumulatively at both concentrations tested, there are only 8 other differentially expressed proteins, however at a much lower significance ($-\log_{10} p < 2.5$).

2.4. Efficient AURKA-degraders potently inhibit NB cell growth and induce apoptosis

To test whether AURKA degradation leads to cell growth inhibition, we treated NGP cells with increasing PROTAC concentrations and monitored cell confluency over time. As shown at the 48h timepoint, PROTACs **SK3251** (IC_{50} 80.8 nM), **SK2188** (IC_{50} 31.9 nM) and **SK2189** (IC_{50} 50.9 nM) potently inhibit cell growth and significantly outperform the parent inhibitor MK-5108 (IC_{50} 361.7 nM) (Fig. 5A and Supplementary Fig. S2A). As expected, the opposite is true for **SK3250** (IC_{50} 1311.0 nM) which failed to induce AURKA degradation. The potency of **SK2186** and **SK2187**, which feature an additional amide group, is slightly lower compared to that of **SK2188** and **SK2189** with similar linker lengths. The alisertib-based PROTAC **JB170** (IC_{50} 876.6 nM) is much less potent and even fails to outperform AURKA inhibitor MK-5108. As expected, the inactive degrader analogue **SK3288** displayed very weak antiproliferative effects.

To assess induction of apoptosis by lead compound **SK2188**, we used the CaspaseGlo™ 3/7 Assay following 24h treatment in NGP (Fig. 5B). While MK-5108 caused a significant increase in caspase 3/7 activity at 1000 nM ($p \leq 0.0001$), **SK2188** outperformed its parent inhibitor with significant induction of apoptosis starting from as low as 10 nM ($p \leq 0.05$).

2.5. Degradation of AURKA with SK2188 induced elevated markers for replicative stress and associated DNA damage

To further evaluate the benefits of AUKRA degradation over inhibition, we directly compared downstream effects of **SK2188** and MK-5108 (Fig. 5C). Immunoblotting after 24h confirms the previously shown upregulation of AURKA upon MK-5108 treatment and the potent degradation by **SK2188** which, as expected, is selective for AURKA over AURKB. Additionally, we confirm the previously established secondary reduction of MYCN and observe this to be a dose-dependent effect. Interestingly, degradation of AURKA with **SK2188** induced elevated markers for replicative stress and associated DNA damage, as measured by pCHK1-, pRPA32-and - γH2AX -levels.

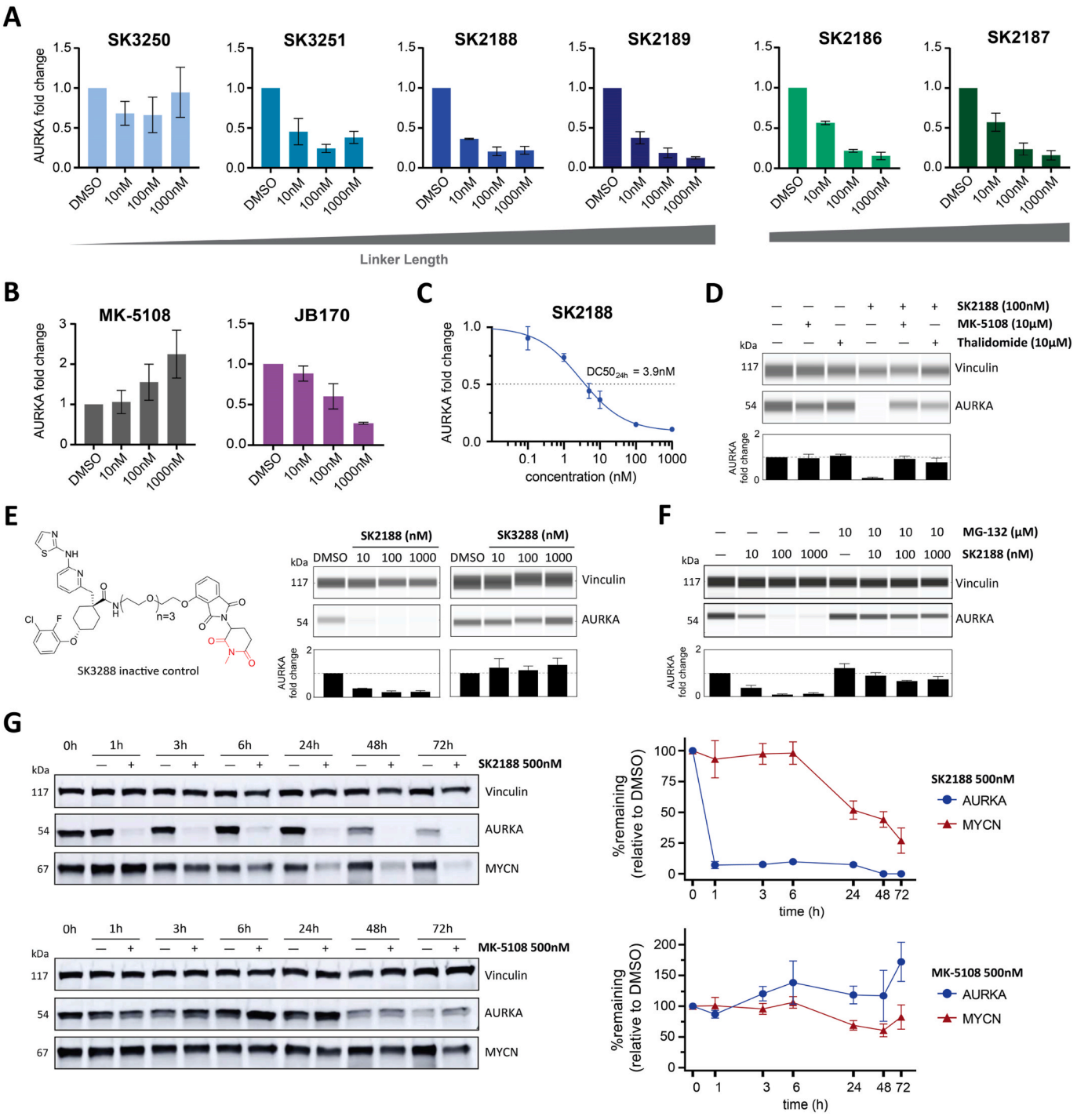

Fig. 3. PROTAC SK2188 induces potent AURKA degradation and subsequent reduction of MYCN in NGP neuroblastoma cells. (A) Simple Western analyses of AURKA after 24h treatment with indicated concentrations of MK-5108-based PROTACS, **(B)** parent inhibitor MK-5108 and previously reported alisertib-based PROTAC JB170, using vinculin as loading control. Bars represent quantification of Simple Western data (Supplementary Fig. S2B), displayed as mean AURKA fold changes relative to DMSO-treated controls ± SD (n = 3). **(C)** Dose-response curve and $DC_{50,24h}$ derivation of SK2188 following similar Simple Western analyses as (**3A-3B**), using a larger concentration range as indicated (Supplementary Fig. S2C). **(D)** Simple Western of AURKA in cells treated with indicated combinations of SK2188, MK-5108 and thalidomide. Bars represent quantification of Simple Western data (mean ± SD, n = 3). **(E)** Chemical structure of SK3288 (left) and Simple Western of AURKA comparing 24h treatment with SK2188 and SK3288 (right) along with their quantifications (mean ± SD, n = 3). **(F)** Simple Western and quantification of AURKA fold changes following 1h treatment with SK2188 with or without the presence of proteasome inhibitor MG-132 (mean ± SD, n = 3). **(G)** Western blots of AURKA and MYCN (left) following treatment with 500 nM of SK2188 and MK-5108 in a time-series assay, using vinculin as loading control. Linear plots (right) display quantification of the Western blot data showing percentage of protein remaining relative to the DMSO control of their respective timepoints (n = 3).

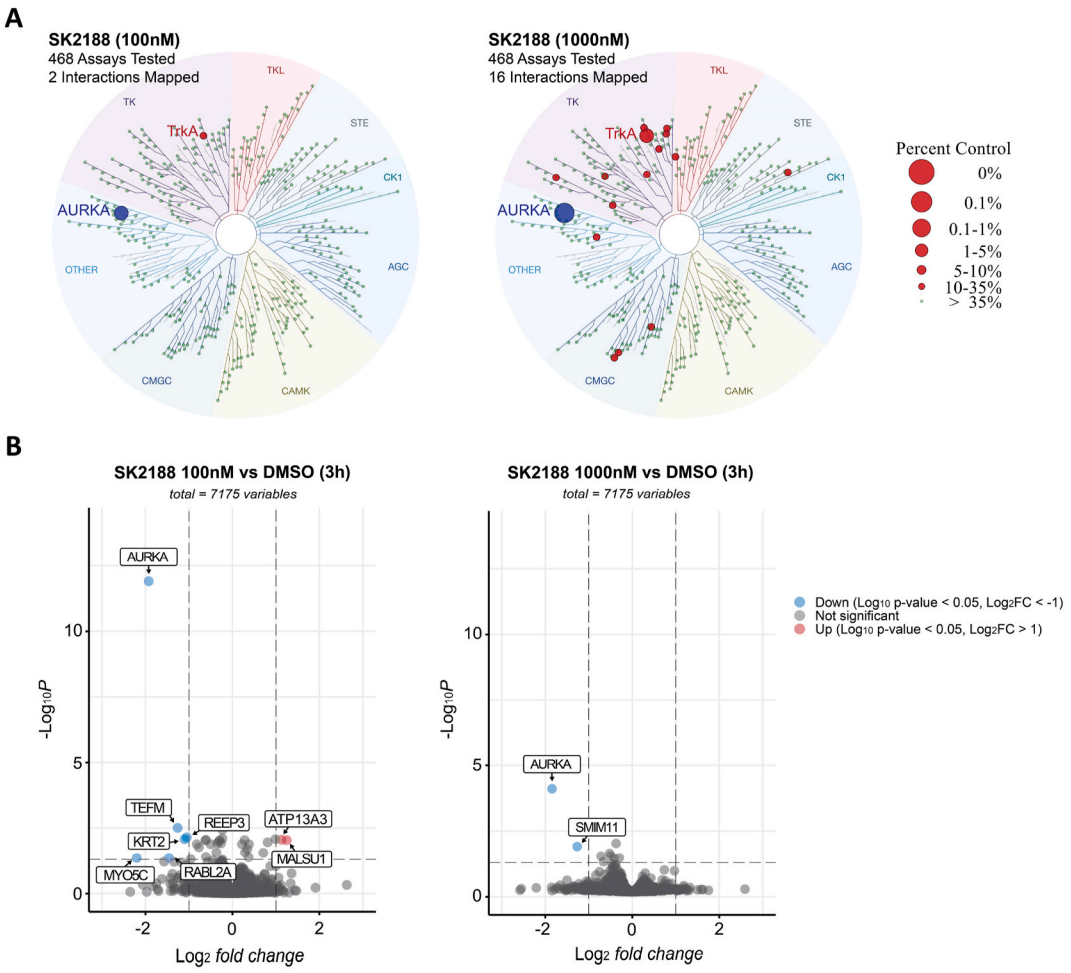

Fig. 4. PROTAC SK2188 displays high AURKA binding selectivity and limited off-target degradation. (A) KINOMEscan TREEspot map analyzing the binding-selectivity profile of **SK2188** at 100 nM and 1000 nM against a panel of 468 kinases. **(B)** Shotgun proteome profiling to assess degradation selectivity of **SK2188** at 100 nM and 1000 nM following 3h treatment in NGP.

2.6. SK2188 anti-proliferative activity varies across NB cell lines and patient-derived organoids

To determine the anti-proliferative activity of **SK2188** in other NB cell lines, we additionally evaluated cell growth inhibition of MK-5108 and **SK2188** in IMR-32 (*MYCN* amplified), N206 (*MYCN* amplified) and SK-N-AS (*MYCN* non-amplified) (Fig. 5D). MK-5108 showed the highest potency in NGP and IMR-32, while it was slightly less effective in SK-N-AS and N206. On the other hand, PROTAC **SK2188** showed a 10-fold higher potency in NGP and IMR-32 with IC_{50}-values of 31.9 and 21.5 nM respectively, while unable to outperform the parent inhibitor MK-5108 in N206 and SK-N-AS.

To further explore the clinical potential of AURKA-degraders, we evaluated the effects of **SK2188** on cell viability in 4 patient-derived NB organoids (Fig. 5E). In NB139 (*MYCN* non-amplified) and NB067 (*MYCN* amplified), **SK2188** showed superior activity to MK-5108 with IC_{50} values of 131.3 and 26.4 nM respectively. In contrast, **SK2188** was less potent in 000GKX (*MYCN* amplified) and showed almost no activity in NB059 (*MYCN* non-amplified).

3. Shorter linker length is tolerated in the regioisomeric 5-substituted PROTAC series

As the PROTACs discussed above displayed promising activity, we explored the possibility of switching the linker attachment point from the 4- to the 5-position of thalidomide. Relative to **SK3251**, **SK2188** and **SK2189**, the regioisomeric 5-substituted PROTACs **SK3278**, **SK3286** and **SK3287** exhibited similar degradation profiles with $D_{max,24h}$ values of ±85% (Fig. 6A). Strikingly, in contrast to **SK3250** which failed to degrade AURKA, switching the PEG2 linker to the 5-position (**SK3277**) reduced AURKA levels to 45% and 17% at 10 nM and 100 nM, respectively. Further increasing the concentration to 1000 nM resulted in reduced target degradation, indicating a typical hook-effect. All 5-substituted PROTACs also showed strong antiproliferative effects in NGP (Fig. 6B).

4. Discussion

Inhibition of AURKA is actively being pursued as a therapeutic modality in neuroblastoma due to its catalytic role in mitosis as well as its kinase-independent functions regulating MYCN protein stability, DNA damage repair and mediation of replicative stress. However, the use of small-molecule inhibitors primarily target AURKA's kinase-related functions in mitosis. In addition, we and others have observed a strong upregulation of AURKA upon treatment with classical inhibitors, which could potentially be associated with therapy resistance in the clinic. In this respect, we successfully designed and synthesized MK-5108-based PROTACS capable of degrading AURKA at low nanomolar concentrations in a neuroblastoma context. The most potent compound, **SK2188**, is capable of degrading AURKA with a $DC_{50,24h}$ value of 3.9 nM in a proteasome- and E3-ligase dependent manner. Furthermore, degradation kinetics at 500 nM revealed very rapid activity with ~93%

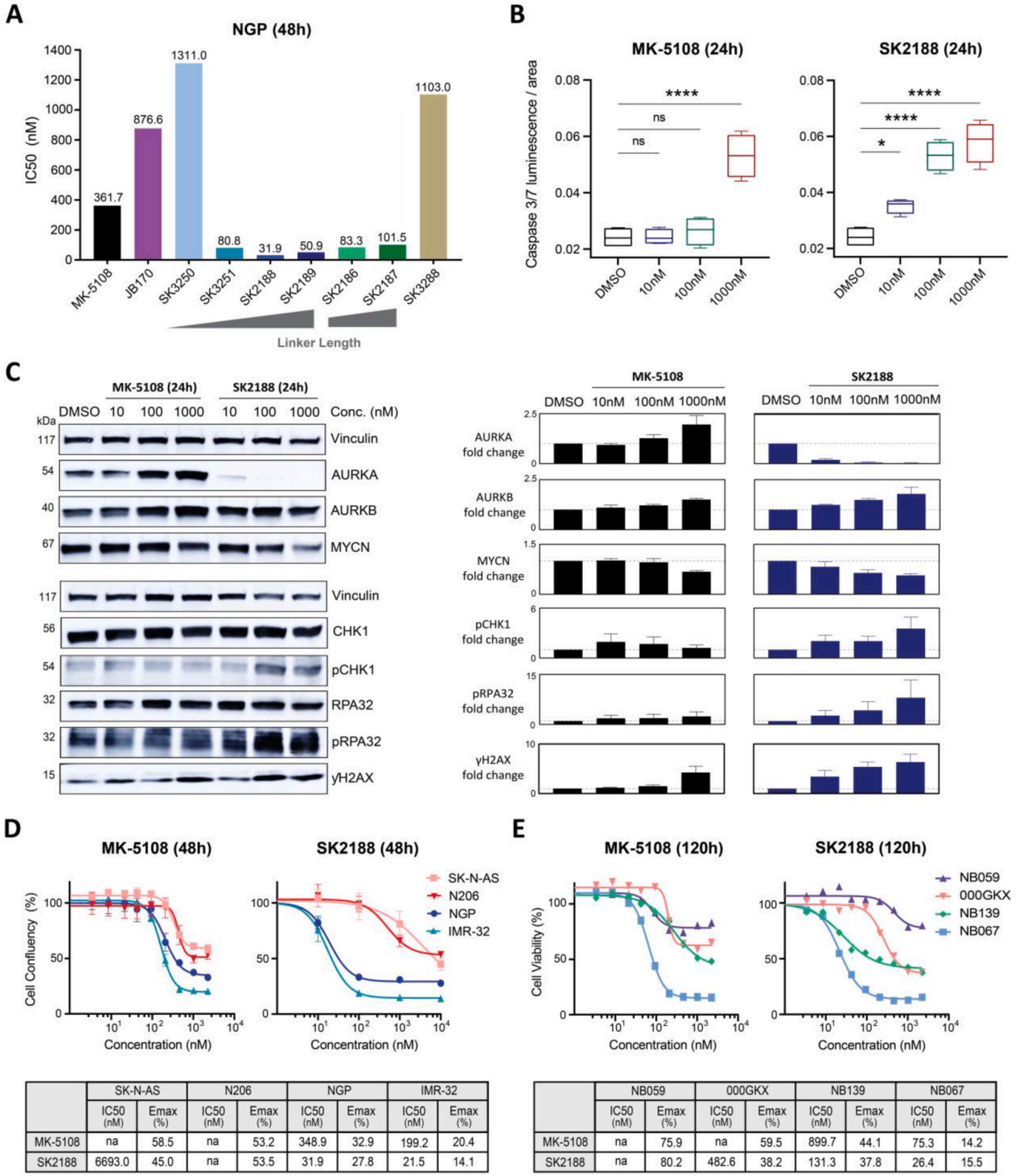

	SK-N-AS		N206		NGP		IMR-32	
	IC50 (nM)	Emax (%)	IC50 (nM)	Emax (%)	IC50 (nM)	Emax (%)	IC50 (nM)	Emax (%)
MK-5108	na	58.5	na	53.2	348.9	32.9	199.2	20.4
SK2188	6693.0	45.0	na	53.5	31.9	27.8	21.5	14.1

	NB059		000GKX		NB139		NB067	
	IC50 (nM)	Emax (%)	IC50 (nM)	Emax (%)	IC50 (nM)	Emax (%)	IC50 (nM)	Emax (%)
MK-5108	na	75.9	na	59.5	899.7	44.1	75.3	14.2
SK2188	na	80.2	482.6	38.2	131.3	37.8	26.4	15.5

Fig. 5. PROTAC SK2188 inhibits NB cell growth, triggers apoptosis and results in elevated DNA damage and replicative stress markers. (A) Incucyte® Live-Cell monitoring of NGP treated with a concentration range (10-10,000 nM) of indicated compounds. Bars represent absolute $IC_{50,\ 48h}$ derived from dose-response curves (n = 4) (Supplementary Fig. S2A). **(B)** Caspase-Glo® 3/7 Assays showing induction of apoptosis by MK-5108 and SK2188 in NGP after 24h treatment, represented as caspase 3/7 signal per cell-occupied area. Whiskers represent minimum and maximum values between 4 biological replicates. Significance was measured using one-way ANOVA with Dunnet's Multiple Comparisons Test (* = $p \leq 0.05$, **** = $p \leq 0.0001$, ns = non-significant). **(C)** Western blot of indicated proteins in NGP after 24h treatment with MK-5108 and SK2188, using vinculin as loading control. Bars represent quantification of Western blot data (mean ± SEM, n = 3). **(D)** Dose-response curves of MK-5108 and SK2188 evaluated across NB cell lines using Incucyte® Live-Cell Imaging (n = 4) and **(E)** in NB patient-derived organoids using CellTiter-Glo® (n = 1). Corresponding absolute $IC_{50,\ 48h}$ and $E_{max,\ 48h}$ values are displayed.

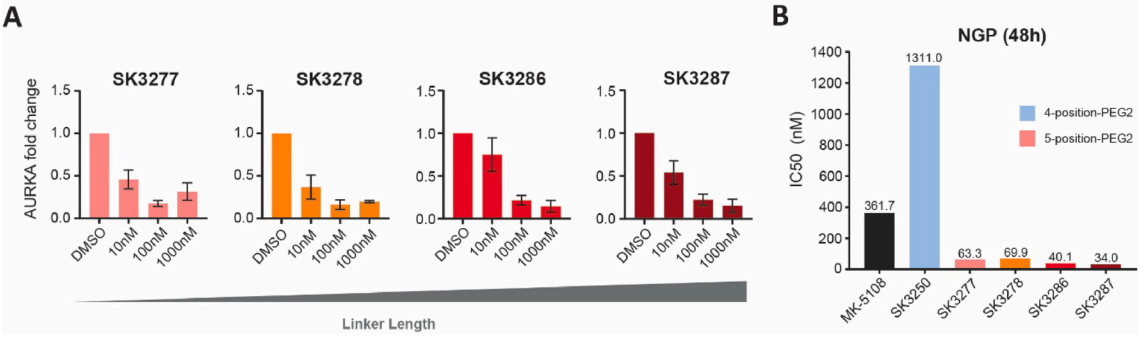

Fig. 6. MK-5108-based PROTAC with shorter linker length is better tolerated at the 5-position of thalidomide. (A) Simple Western of AURKA in NGP treated for 24h with indicated concentrations of MK-5108-based PROTACS, using vinculin as loading control. Bars represent mean AURKA fold changes ± SD from 3 biological replicates (Supplementary Fig. S2B). **(B)** IncuCyte® Live-Cell monitoring of NGP treated with a concentration range (10-10,000 nM) of indicated compounds. Bars represent absolute $IC_{50,\ 48h}$ values derived from dose-response curves (n = 4) (Supplementary Fig. S2A).

degradation of AURKA after 1h and complete degradation at 48h, indicating quick and sustained PROTAC activity. Remarkably, a kinome-wide scan revealed very little off-target binding of PROTAC **SK2188**, which only binds AURKA and TrkA at 100 nM. In addition, differential protein expression analysis using shotgun proteome profiling revealed selective AURKA degradation by **SK2188** at 100 and 1000 nM with limited effect on other proteins. Importantly, we observe the absence of prototypical off-target proteins (e.g., GSPT1, ZFP91 & ZNF653) which are commonly degraded by thalidomide/pomalidomide-based PROTACs via a molecular glue-type mechanism [37], indicating excellent degradation selectivity of **SK2188**.

Interestingly, we observe that AURKA degradation by PROTAC **SK2188** was associated with reduced MYCN levels in a time- and dose-dependent manner. More specifically, instant and sustained degradation of AURKA ultimately resulted in the subsequent reduction of MYCN up to 73% after 72h treatment. Furthermore, relative to MK-5108, **SK2188** efficiently induces replicative stress and DNA damage, and causes apoptosis at low nanomolar concentrations. All these data further support the benefits of targeted AURKA degradation as opposed to conventional inhibition as a therapeutic option for neuroblastoma.

Furthermore, compared to MK-5108, antiproliferative effects of AURKA PROTACs were significantly enhanced in NGP and IMR-32. Likewise, **SK2188** strongly reduced cell viability in patient-derived organoids NB067 and NB139, demonstrating the clinical potential for AURKA-degraders in a neuroblastoma context. Interestingly, we observed that sensitivity to AURKA degradation by PROTAC **SK2188** does not seem to be dependent on MYCN amplification status but may instead be correlated to baseline levels of AURKA and/or CRBN. The antiproliferative effects in N206 and SK-N-AS, for instance, are less pronounced than in NGP and IMR-32, which could be related to higher baseline levels of AURKA and/or relatively lower expression of CRBN (Supplementary Fig. S1C), but requires further investigation.

Finally, we explored regioisomeric PROTACs in which thalidomide was connected via position 5 instead of 4. Interestingly, analogue **SK3250** (2 PEG units, position 4) failed to deplete AURKA and displayed poor anti-proliferative activity. In contrast, altering the exit position from the 4- to the 5-position allowed us to identify a potent degrader (57% degradation at 10 nM) that features a short PEG 2-linker, i.e., **SK3277**. This observation demonstrates how changing the exit vector may allow to uncover degraders with reduced molecular weight, a smaller number of rotational bounds (nRoB) and lower TPSA, physicochemical features that are believed to facilitate further development [22,34,38]. In addition, shorter linkers have been shown to be more metabolically stable due to fewer soft spots and more steric hindrance of target and E3-ligase ligand, discouraging binding to metabolizing enzymes [39].

In summary, our data highlights the therapeutic potential of MK-5108-based PROTACS in a neuroblastoma context, which degrade AURKA at low nM potency. Similar to very recent observations by Knapp et al. [19], MK-5108-based PROTACS with PEG linkers attached onto the 4-position of thalidomide significantly outperform previously existing alisertib-based PROTAC **JB170**. Interestingly though, while PROTAC **JB325** (= **SK2188** in our study) showed only weak in-cell AURKA binding as observed via a nanoBRET assay (EC_{50} 1390 nM), this lead compound resulted in strongly reduced AURKA levels and displayed low nM cell growth inhibition in our live-cell assays. Unfortunately, we are not able to compare degradation and cell proliferation data since these were not published for **JB325.** Additionally, around a 10-fold difference in degradation potency and cell viability was observed between **JB301** (= **SK2187**) and **JB300** (=**SK2186**), while in NGP we found both PROTACs to exhibit similar potency. Compared to PROTAC **HLB-0532259** of a recent preprint [18], designed to target the AURKA/MYCN complex, our PROTAC series seem equipotent AURKA degraders and show similar antiproliferative effects in neuroblastoma. Finally, we report novel MK-5108-based PROTACs by switching the linker attachment point onto the 5-position of thalidomide, which led to the discovery of a potent degrader with a short linker length interesting for further optimization and validation.

5. Chemistry

The synthesis of MK-5108 was performed based on a reported procedure [40]. Synthetic schemes and experimental details can be found in the supporting information. 4-Hydroxythalidomide [41] was alkylated with *tert*-butyl bromoacetate in very good yield. Hydrolysis of the *tert*-butyl ester followed by classical HATU-amide formation delivered **2** and **3**. Direct alkylation of 4-hydroxy thalidomide with tosylated or mesylated linkers was sluggish and suffered from difficult separations and moderate yields (data not shown), in line with literature data [42,43]. This led us to explore *O*-alkylation under Mitsunobu conditions. We optimized the protocol by using excess of 4-hydroxythalidomide (1.1 eq) and the linker as limiting reagent (1.0 eq). Excess 4-hydroxythalidomide could easily be removed by performing 2 washing steps with sat. $NaHCO_3$ and removal of the formed triphenylphosine oxide via column chromatography, affording the desired products **4**–**7** in excellent yields. Glutarimide substitution was not observed. A similar Mitsunobu protocol was used to pegylate 5-hydroxythalidomide and yielded products **8**–**11**. However, here around 20% of glutarimide alkylation was observed, resulting in more sluggish purifications and lower yields. After Boc deprotection of the thalidomide reagents, the final PROTACs were synthesized using HATU-mediated amide coupling with yields ranging from 62 to 89% (Scheme 1).

A methylated glutarimide ring analogue of PROTAC SK2188 was synthesized as a negative control [44]. Typically, the synthesis of such inactive analogues starts with methylation of a NHBoc-glutarimide or thalidomide building block, followed by PROTAC construction [43].

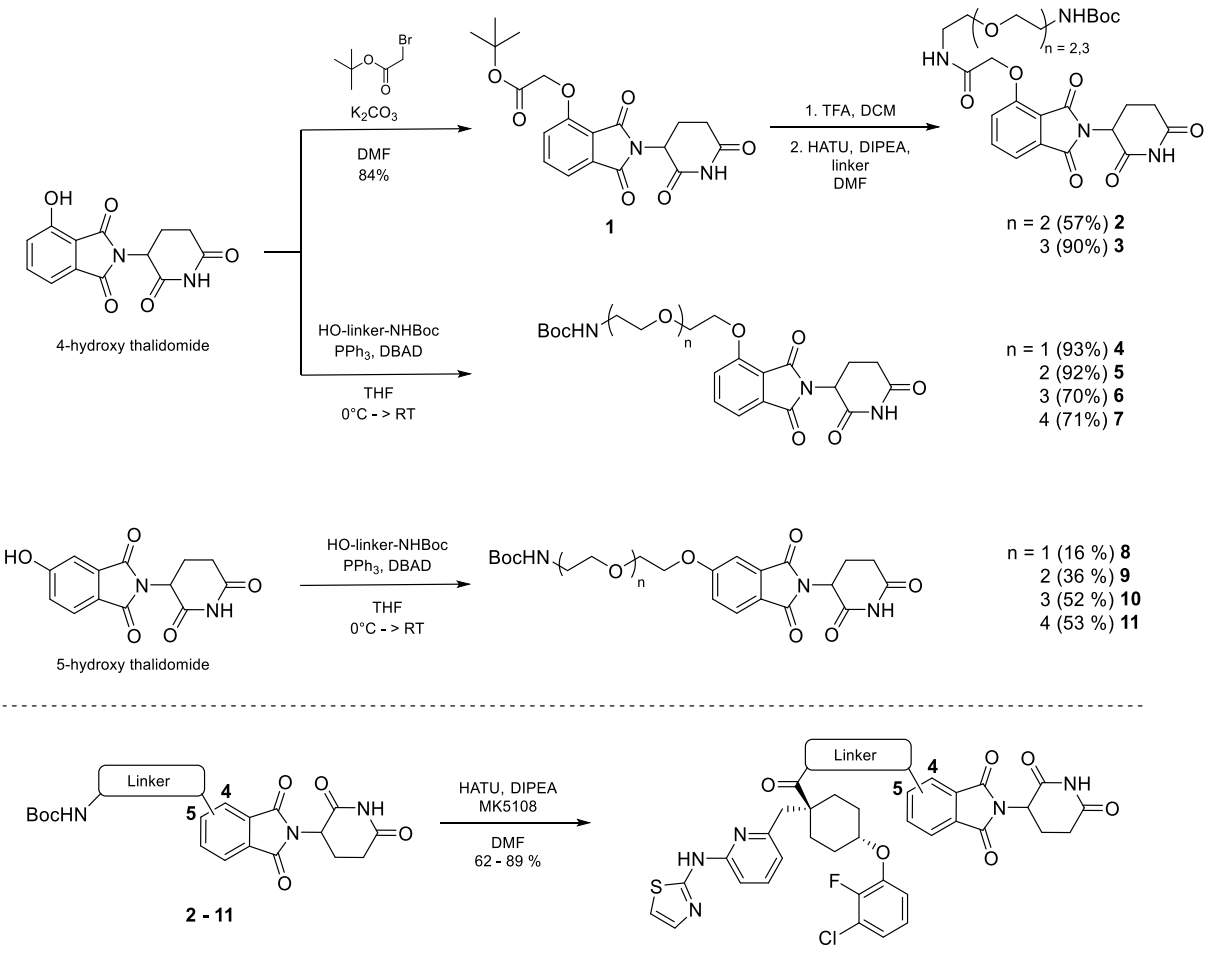

Scheme 1. Synthesis of intermediates **2**–**11** and final PROTACs.

However, we found that it is possible to perform the methylation on a more advanced PEGylated thalidomide under Mitsunobu conditions. Final HATU-coupling resulted in inactive control **SK3288** (Scheme 2).

6. Experimental section

Cell culture and organoids. Human NB cell lines NGP, IMR-32, SK-N-AS and N206 were either bought commercially (DSMZ and ATCC) or obtained through research laboratories. Cells were cultured in RPMI 1640 medium supplemented with 10% fetal calf serum, 2 mM L-glutamine and 100 IU/mL penicillin/streptomycin. Screening for mycoplasma contamination occurred routinely on the cells. Patient-derived NB organoids 000GKX, NB059, NB067 and NB139 were a gift from the Molenaar Lab at the Prinses Máxima Center (Utrecht, the Netherlands). Further molecular information on the organoids can be found in Supplementary Table S3. The composition of the growth medium used (further referred to as NB OM) can be found in Supplementary Table S4. Incubation of both cells and organoids occurred at 37 °C and 5% CO_2.

Protein extraction from cells. To monitor changes in AURKA protein levels, NGP cells were seeded in T-25 flasks at a density of ~2 × 10^6 cells/flask and allowed to adhere for 48h. Afterwards, treatment was done by medium replacement containing the compound of interest in its corresponding concentration. All samples were normalized to contain the same percentage of DMSO as the controls. Cells were harvested at their respective time points using scrapers (VWR), washing with ice-cold PBS (Life technologies) and concomitant centrifugation steps at 1000×*g*. In co-treatment experiments, cells were first pre-treated with MG-132 (Merck Millipore), MK-5108 or thalidomide at 10 μM for 1h by shaking gently at room temperature prior to addition of SK2188. Afterwards, similar procedures were followed for cell harvesting. All collected cell pellets were lysed in cold RIPA buffer (0.5% w/v Sodium Deoxycholate, 150 mM NaCl, 50 mM TrisHCl pH7.5, 0.1% w/v SDS, 1%

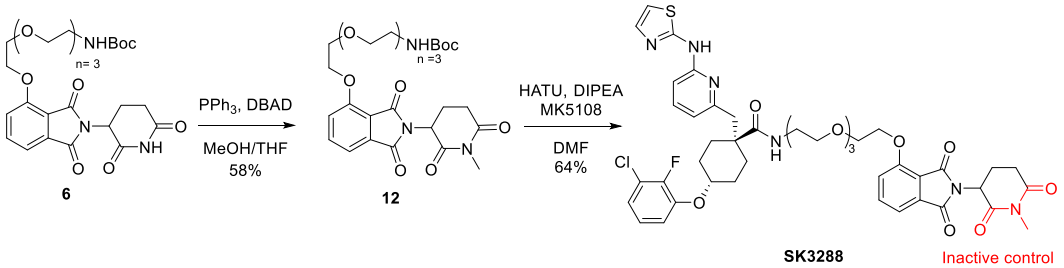

Scheme 2. Synthesis of inactive analogue **SK3288**.

w/v NP-40) supplemented with protease and phosphatase inhibitors (Roche) by rotating at 4 °C for 1h. Concentrations of the obtained protein lysates were measured using the Pierce™ BCA Protein Assay Kit (ThermoFisher). Time points used were 24h for the initial PROTAC screening and the further comparisons between SK2188 and MK-5108, 1h for the co-treatment experiments and various timepoints for the time-series (0h, 1h, 3h, 6h, 24h, 48h and 72h).

Simple Western analysis. Simple Western analyses were performed with the Wes instrument (Bio-Techne) [35] using the 12–230 kDa Wes Separation module and the EZ standard pack reagent 1 (Protein Simple) under denaturing conditions. Protein lysates were loaded at 0.8 μg/μL and antibodies were used for detection of AURKA and vinculin. Origin and dilutions of the antibodies can be found in Supplementary Table S6. Chemiluminescence peaks were generated by the Compass Software for Simple Western and the area calculated using the gaussian fit method. Area of the peaks corresponding to AURKA were normalized to those of vinculin and fold changes were calculated relative to DMSO controls.

Western blotting. Protein lysates were denatured through addition of Laemli buffer supplemented with β-mercaptoethanol heated at 95 °C for 10 min (Supplementary Table S7). Samples were subsequently loaded on 10% Mini-Protean TGX Precast Gels (Bio-Rad) with a total protein input mass of 35 μg and run at 120V for 1h under 10x Tris/glycine/SDS buffer. Afterwards, proteins were blotted on nitrocellulose membranes by running at 100V for 1 h with a buffer containing 10% 10x Tris/glycine and 20% methanol. Ponceau staining was used for confirmation of protein transfer. Membranes were blocked in 5% milk/TBST or 5% BSA/TBST for 1h at room temperature and subsequently incubated with primary antibodies overnight at 4 °C. Blots were washed 3 × 5 min with TBST prior to incubation with secondary antibodies for 1h at room temperature. Visualization of the blots was done using WestDura or WestFemto (ThermoFisher) with the Amersham™ Imager 680 (BIOKÉ). Blots were stripped using the Restore™ Stripping Buffer (ThermoFisher) prior to detection of additional proteins. Quantification of corresponding bands occurred via ImageJ and fold changes were calculated relative to DMSO controls following vinculin normalization. Primary antibodies used were AURKA, AURKB, MYCN, γH2AX, CHK1, p-CHK1, RPA32, p-RPA32 and vinculin (Supplementary Table S6).

Cell confluency assay. Cells were seeded at 4500 (NGP, IMR-32 & N206) or 2100 cells per well (SK–N-AS) in Corning™ 384-well plates and allowed to adhere overnight. Compound treatment was performed using the Tecan D300e Digital Dispenser at a range of concentrations in triplicate and cell confluency was monitored over time using the IncuCyte® Live-Cell Imaging System. Percentage confluence data at 48h was normalized to the DMSO control using the in-house developed program HTSplotter [45]. Area under the curve (AUC) and absolute half-maximal inhibitory (IC_{50}) values were calculated using GraphPad Prism Software (version 9.3.1). Dose-response curve analyses were computed using the variable slope (four parameters) equation.

Organoid viability assay. Patient-derived organoids 000GKX, NB059, NB067 and NB139 were centrifuged at 250G at 8 °C for 5 min, the NB OM aspirated and 1 ml of Accutase™ added to the cell pellet. 1 ml of Accutase™ was added to the culture vessels of 000GKX and NB139 as these organoids grow in partial attachment to the culture vessel. Accutase™ was diluted with 4 ml NB OM and organoids were passed through FACS tube filters and visualized under a microscope to ensure single cell suspension. Cells were counted using the Bio-Rad Trypan Blue cell counting kit and plated in Corning™ 384-well plates using the Thermo Scientific™ Multidrop™ Combi Reagent Dispenser. The seeding density of 000GKX, NB059, NB067 and NB139 in the 384-well plates were 5000, 20000, 5000 and 3000 cells per well respectively as previously determined in growth curve CellTiter-Glo® 3D (CTG3D) cell viability assays. After 24 h, MK-5108 and SK2188 were administered in a concentration range in triplicate using the Tecan D300e Digital Dispenser. Wells were normalized to contain the same DMSO percentage as controls. Organoids were incubated at 37 °C and 5% CO_2 for 120 h. Organoids were then treated with CTG3D according to manufacturer's guidelines and absorbance was measured using the SpectraMax® i3x Multi-Mode Microplate Reader.

Apoptosis induction analysis. NGP cells were seeded at 25,000 cells per well in Corning™ 96-well plates and allowed to adhere overnight. Drugging was performed using the Tecan D300e Digital Dispenser in triplicate with each well containing the same DMSO percentage as controls. At the 24h timepoint, one scan was performed with the IncuCyte® Live-Cell Imaging System and cell-occupied area values (μm^2) were derived per well. Directly after, a Caspase-Glo® 3/7 Assay (Promega) was performed using the GloMax® Discover Microplate Reader for detection. The protocol was adapted to add 50 μL of caspase reagent per well. The average relative light units (RLU) of each well was normalized to the cell-occupied area. To assess significance, one-way ANOVA with Dunnet's Multiple Comparisons Tests were performed using GraphPad Prism Software (version 9.3.1). Statistical significance was determined with a p-value of 0.05 or smaller (* = $p \leq 0.05$, **** = $p \leq 0.0001$, ns = non-significant).

Kinome scan. The kinome scan was performed by Eurofins Scientific's *scan*MAX® screening platform.

6.1. Shotgun proteomics

Sample preparation. Cell pellets were homogenized in 200 μl lysis buffer containing 5% sodium dodecyl sulfate (SDS) and 50 mM triethylammonium bicarbonate (TEAB), pH 8.5. Next, the resulting lysate was transferred to a 96-well PIXUL plate in 100 μl aliquots and sonicated with a PIXUL Multisample sonicator (Active Motif) for 10 min with default settings (Pulse 50 cycles, PRF 1 kHz, Burst Rate 20 Hz). After centrifugation of the samples for 15 min at maximum speed at room temperature (RT) to remove insoluble components, the protein concentration was measured by bicinchoninic acid (BCA) assay (Thermo Scientific) and from each sample 100 μg of protein was isolated to continue the protocol. Proteins were reduced by addition of 15 mM dithiothreitol and incubation for 30 min at 55 °C and then alkylated by addition of 30 mM iodoacetamide and incubation for 15 min at RT in the dark. Phosphoric acid was added to a final concentration of 1.2% and subsequently samples were diluted 7-fold with binding buffer containing 90% methanol in 100 mM TEAB, pH 7.55. The samples were loaded on a 96-well S-Trap™ plate (Protifi) and a Resolvex® A200 positive pressure workstation (Tecan Group Ltd) was used for semi-automatic processing. After protein binding, the S-trap™ plate was washed three times with 200 μl binding buffer. A new deepwell plate was placed below the 96-well S-Trap™ plate and trypsin (1/100, w/w) was added for digestion overnight at 37 °C. Also using the Resolvex® A200 workstation, peptides were eluted in three times, first with 80 μl 50 mM TEAB, then with 80 μl 0.2% formic acid (FA) in water and finally with 80 μl 0.2% FA in water/acetonitrile (ACN) (50/50, v/v). Eluted peptides were dried completely by vacuum centrifugation. Peptides were redissolved in loading solvent A (0.1% TFA in water/acetonitrile (ACN) (98:2, v/v)) and desalted on a reversed phase (RP) C18 OMIX tip (Agilent). The tip was first washed 3 times with 100 μl pre-wash buffer (0.1% TFA in water/ACN (20:80, v/v)) and pre-equilibrated 5 times with 100 μl of wash buffer (0.1% TFA in water) before the sample was loaded on the tip. After peptide binding, the tip was washed 3 times with 100 μl of wash buffer and peptides were eluted twice with 100 μl elution buffer (0.1% TFA in water/ACN (40:60, v/v)). The combined elutions were transferred to HPLC inserts and dried in a vacuum concentrator.

LC-MS/MS analysis. Peptides were re-dissolved in 20 μl loading solvent A (0.1% trifluoroacetic acid in water/acetonitrile (ACN) (98:2, v/v)) of which 5 μl was injected for LC-MS/MS analysis on an Ultimate 3000 RSLCnano system in-line connected to a Q Exactive HF mass spectrometer (Thermo). Trapping was performed at 10 μl/min for 2 min in loading solvent A on a 5 mm trapping column (Thermo scientific, 300 μm internal diameter (I.D.), 5 μm beads). The peptides were separated on a 250 mm Aurora Ultimate, 1.7 μm C18, 75 μm inner diameter (Ionopticks) kept at a constant temperature of 45 °C. Peptides were

eluted by a non-linear gradient starting at 1% MS solvent B reaching 33% MS solvent B (0.1% FA in water/acetonitrile (2:8, v/v)) in 100 min, 55% MS solvent B (0.1% FA in water/acetonitrile (2:8, v/v)) in 135 min, 70% MS solvent B in 145 min followed by a 10-min wash at 70% MS solvent B and re-equilibration with MS solvent A (0.1% FA in water). The mass spectrometer was operated in data-independent mode, automatically switching between MS and MS/MS acquisition. Full-scan MS spectra ranging from 375 to 1500 m/z with a target value of 5E6, a maximum fill time of 50 ms and a resolution at of 60,000 were followed by 30 quadrupole isolations with a precursor isolation width of 10 m/z for HCD fragmentation at an NCE of 30% after filling the trap at a target value of 3E6 for maximum injection time of 45 ms. MS2 spectra were acquired at a resolution of 15,000 at 200 m/z in the Orbitrap analyser without multiplexing. The isolation intervals ranging from 400 to 900 m/z, without overlap were created with the Skyline software tool. QCloud [46] as used to control instrument longitudinal performance during the project.

Data analysis. LC-MS/MS runs of all samples were searched using the library free DiaNN algorithm (version 1.8.1) [47]. Samples from each time point of incubation with PROTAC were analyzed separately. Spectra were searched against the human protein sequences in the Swiss-Prot database (database release version of 2022_01), containing 20,588 sequences (www.uniprot.org). Enzyme specificity was set as C-terminal to arginine and lysine, also allowing cleavage at proline bonds with a maximum of two missed cleavages. Variable modifications were set to oxidation of methionine residues and acetylation of protein N-termini. Mainly default settings were used, except for the addition of a 375–900 m/z precursor mass range filter, the match between runs (MBR) option. Further data analysis of the results was performed with an in-house R script [48], using the main report file output table from DiaNN. After selection of protein groups containing at least one proteotypic peptide and application of a 1% 'Lib.PG.Q.Value' cutoff filter, MaxLFQ intensities were log2 transformed and replicate samples were grouped. Proteins with less than two valid values in at least one group were removed and missing values were imputed from a normal distribution centered around the detection limit (package DEP [48]), leading to a list of 7175 and 7097 quantified proteins in the 3h and 24 experiment, respectively, which were used for further data analysis. To compare protein abundance between pairs of sample groups (SK2188 100 nM vs DMSO, SK2188 100 nM vs DMSO and SK2188 1000 nM vs SK2188 100 nM), statistical testing for differences between two group means was performed, using the package limma [49]. Statistical significance for differential regulation was set to a false discovery rate (FDR) of <0.05 and fold change of >2- or <0.5-fold (|log2FC| = 1).

Analysis & Figures. Apart from Figs. 1 and 2 (ChemDraw), all graphs were generated using GraphPad Prism Software (version 9.3.1) and compiled with Adobe Illustrator (2022). Unless otherwise stated, data are expressed as mean ± SD from three or more biological replicates.

6.2. Chemistry

General. All solvents utilized were used as received, were purchased from Chemlab (Zedelgem, Belgium), and were of HPLC grade or equivalent or superior purity. All building blocks and reagents were used as received and were purchased from common chemical suppliers including but not limited to: Fluorochem (Glossop, Derbyshire UK), Apollo Scientific (Bredbury/Stockport Cheshire UK), Sigma-Aldrich (Diegem, Belgium), and Fisher Scientific (Merelbeke, Belgium). All reactions described were performed in a fume hood. Additionally, all reactions were carried out under a nitrogen atmosphere and at room temperature (ca 21 °C) unless explicitly stated otherwise. Reactions were monitored by TLC or analytical LCMS. Analytical TLC was performed on Machery-Nagel precoated F254 aluminum plates and visualed under UV light (254 nm) and/or via staining the plates with basic aq. KMnO4, cerium-molybdate, or sulfuric acid-anisaldehyde spray. LC-MS analysis were carried out on a Waters Autopurification system equipped with a Waters CORTECS column (4.6 × 100 mm, C18, 2.7 μm) and using a water/acetonitrile/trifluoroacetic acid linear gradient. Peak detection was achieved using mass spectrometry (ESI-MD) and a photo-diode-array detector (PDA). Column chromatography was performed on a Reveleris X2 automated flash chromatography system (Grace/Büchi) using disposable 60 Å silica gel cartridges (Agela). Nuclear magnetic resonance analyses including ^{1}H- and ^{13}C- spectra were carried out on a Bruker Avance Neo 400 MHz spectrometer equipped with an autosampler and using TOPSPIN/ICON-NMR. Chemical shifts are given in ppm (δ) relative to the solvent peak. NMR solvents included $CDCl_3$ (7.26 ppm in ^{1}H NMR, 77.16 ppm in ^{13}C NMR) or DMSO-d_6 (2.50 ppm in ^{1}H NMR and 39.52 ppm in ^{13}C NMR) and were all purchased from Euriso-Top (Saint Aubin, France). High-resolution mass spectrometry was performed on a Waters Premier XE HRMS system that is calibrated using a solution of Le-enkephalin. Infusion of the analyte into the HRMS system was done as a solution (0.5 ngmL^{-1}) in UPLC grade water and acetonitrile. All obtained final compounds had purity >95%, as assayed by analytical HPLC (UV) using a linear gradient Water/MeCN 0 -> 98% + 0.02% TFA in 10 min on a Waters CORTECS column (4.6 × 100 mm, C18, 2.7 μm).

The synthetic procedures for MK-5108, intermediates **2**–**12**, **SK3288** and **JB170** can be found in the supporting information.

General procedure for PROTAC synthesis (HATU-coupling): The Boc-protected amine (0.12 mmol, 1.2 eq) was dissolved in DCM (2 ml) and TFA (1 ml) and stirred for 1.5 h. Then, the volatiles were evaporated. MK-5108 (50 mg, 0.10 mmol, 1.0 eq) and HATU (46 mg, 0.12 mmol, 1.2 eq) were dissolved in DMF (2 ml), DIPEA (0.087 ml, 5 eq) was added and stirred for 5 min. Then, the amine was dissolved in DMF (2 ml) and added to the activated acid. After approximately 30 min, the RM was transferred to a separation funnel with DCM and washed with sat. NaHCO3 (x2) and Brine (x1). The organic phase was dried over Na_2SO_4, filtered and evaporated. Flash column chromatography using DCM/MeOH 0 -> 10% delivered the final products.

*PROTAC **SK2186*** is synthesized following the general protocol for PROTAC synthesis (HATU coupling). The product was obtained as an off-white solid (66 mg) in 73% yield after column chromatography (DCM/MeOH 0 -> 6%). ^{1}H NMR (DMSO-d_6, 400 MHz): δ = 1.58–1.71 (m, 2H), 1.71–1.94 (m, 6H), 2.04 (m, 1H), 2.51–2.64 (m, 2H, overlap with solvent signal), 2.83–2.98 (m, 3H), 3.18 (m, 2H), 3.27–3.42 (m, 4H, overlap with H_2O-signal), 3.43–3.55 (m, 6H), 4.53 (s, 1H), 4.78 (s, 2H), 5.11 (dd, J = 5.3; 12.9 Hz, 1H), 6.63 (d, J = 7.3Hz, 1H), 6.86 (d, J = 8.2Hz, 1H), 6.96 (d, J = 3.6Hz, 1H), 7.05–7.18 (m, 3H), 7.33–7.42 (m, 2H), 7.48 (d, J = 7.2 Hz, 1H), 7.54 (t, J = 7.8 Hz, 1H), 7.63 (t, J = 5.32 Hz, 1H), 7.78 (dd, J = 7.5; 8.3 Hz, 1H), 8.00 (t, J = 5.5Hz, 1H), 11.12 (br s, 2H) ppm. ^{13}C NMR (DMSO-d_6, 100 MHz): δ = 22.02 (CH2), 26.62 (CH2), 28.39 (CH2), 30.96 (CH2), 38.41 (CH2), 38.77 (CH2), 46.61 (C), 46.83 (CH2), 48.82 (CH), 67.51 (CH2), 68.83 (CH2), 68.88 (CH2), 69.50 (CH2), 69.61 (CH2), 74.34 (CH), 108.13 (CH), 110.70 (CH), 116.06 (CH), 116.23 (CH), 116.68 (CH), 116.77 (C), 120.34 (CH), 120.50 (C), 121.84 (CH), 124.94 (d, ^{3}J(C,F) = 4.8 Hz, CH), 133.04 (C), 136.93 (CH), 137.23 (CH), 137.58 (CH), 146.21 (d, ^{2}J(C,F) = 10.1 Hz, C), 148.9 (d, ^{1}J(C,F) = 245.8 Hz, C), 150.70 (C), 154.96 (C), 155.15 (C), 159.86 (C), 165.46 (C), 166.74 (C), 166.92 (C), 169.89 (C), 172.79 (C), 174.17 (C) ppm. ^{19}F NMR (DMSO-d_6, 377 MHz): δ = −136.29 ppm HRMS: $C_{43}H_{46}ClFN_7O_{10}S$ [M+H] calculated: 906.2694, found: 906.2697 HPLC: Purity: 97%

*PROTAC **SK2187*** is synthesized following the general protocol for PROTAC synthesis (HATU coupling). The product was obtained as an off-white solid (73 mg) in 77% yield after column chromatography (DCM/MeOH 0 -> 6%). ^{1}H NMR (DMSO-d_6, 400 MHz): δ = 1.58–1.71 (m, 2H), 1.72–1.94 (m, 6H), 2.04 (m, 1H), 2.51–2.65 (m, 2H, overlap with solvent signal), 2.84–2.95 (m, 3H), 3.19 (m, 2H), 3.27–3.42 (m, 4H, overlap with H2O-signal), 3.42–3.53 (m, 10H), 4.54 (s, 1H), 4.78 (s, 2H), 5.12 (dd, J = 5.3; 12.9 Hz, 1H), 6.63 (d, J = 7.3Hz, 1H), 6.86 (d, J = 8.2Hz, 1H), 6.95 (d, J = 3.6Hz, 1H), 7.06–7.18 (m, 3H), 7.36 (d, J =

3.6Hz, 1H), 7.39 (d, $J = 8.5$Hz, 1H), 7.49 (d, $J = 7.2$ Hz, 1H), 7.54 (t, $J = 7.8$ Hz, 1H), 7.63 (t, $J = 5.6$ Hz, 1H), 7.80 (dd, J = 7.4; 8.5 Hz, 1H), 7.99 (t, $J = 5.5$Hz, 1H), 11.12 (br s, 2H) ppm. ^{13}C NMR (DMSO-d_6, 100 MHz): $\delta = 22.01$ (CH2), 26.62 (CH2), 28.39 (CH2), 30.95 (CH2), 38.40 (CH2), 38.75 (CH2), 46.61 (C), 46.83 (CH2), 48.82 (CH), 67.51 (CH2), 68.82 (CH2), 68.85 (CH2), 69.52 (CH2), 69.62 (CH2), 69.74 (CH2), 69.77 (CH2), 74.36 (CH), 108.09 (CH), 110.67 (CH), 116.06 (CH), 116.17 (CH), 116.71 (CH), 116.77 (C), 120.34 (CH), 120.50 (C), 121.85 (CH), 124.94 (d, ^{3}J(C,F) = 4.8 Hz, CH), 133.04 (C), 136.94 (CH), 137.38 (CH), 137.56 (CH), 146.21 (d, ^{2}J(C,F) = 10.0 Hz, C), 148.92 (d, ^{1}J(C,F) = 245.7 Hz, C), 150.74 (C), 154.97 (C), 155.15 (C), 159.84 (C), 165.45 (C), 166.74 (C), 166.90 (C), 169.88 (C), 172.78 (C), 174.15 (C) ppm. ^{19}F NMR (DMSO-d_6, 377 MHz): $\delta = -136.27$ ppm HRMS: $C_{45}H_{50}ClFN_7O_{10}S$ [M+H] calculated: 950.2956, found: 950.2958 HPLC: Purity: 98.1%

PROTAC ***SK3250*** is synthesized following the general protocol for PROTAC synthesis (HATU coupling). The product was obtained as an off-white solid (64 mg) in 80% yield after column chromatography (DCM/MeOH 0 -> 10%). ^{1}H NMR (DMSO-d_6, 400 MHz): $\delta = 1.58–1.93$ (m, 8H), 1.94–2.03 (m, 1H), 2.50–2.60 (m, 2H, overlap with solvent signal), 2.80–2.93 (m, 3H), 3.22 (q, $J = 5.6$Hz, 2H), 3.50 (t, $J = 5.6$Hz, 2H), 3.77 (m, 2H), 4.33 (m, 2H), 4.48 (br s, 1H), 5.06 (dd, J = 5.4; 12.9 Hz, 1H), 6.61 (d, $J = 7.3$Hz, 1H), 6.84 (d, $J = 8.2$Hz, 1H), 6.95 (d, $J = 3.6$Hz, 1H), 7.06–7.12 (m, 3H), 7.35 (d, $J = 3.6$Hz, 1H), 7.44 (d, $J = 7.2$Hz, 1H), 7.48–7.55 (m, 2H), 7.62 (t, $J = 5.5$Hz, 1H), 7.79 (dd, J = 7.4; 8.4Hz, 1H), 11.09 (s, 1H), 11.11 (s, 1H) ppm. ^{13}C NMR (DMSO-d_6, 100 MHz): $\delta = 21.98$ (CH2), 26.58 (CH2), 28.34 (CH2), 30.92 (CH2), 38.75 (CH2), 46.58 (C), 46.81 (CH2), 48.73 (CH), 68.37 (CH2), 68.76 (CH2), 69.15 (CH2), 74.32 (CH), 108.03 (CH), 110.66 (CH), 115.39 (CH), 116.14 (CH), 116.28 (C), 116.61 (CH), 119.95 (CH), 120.41 (d, ^{2}J(C,F) = 15.1Hz, C), 121.82 (CH), 124.90 (d, ^{3}J(C,F) = 4.9Hz, CH), 133.23 (C), 137.00 (CH), 137.37 (CH), 137.50 (CH), 146.19 (d, ^{2}J(C,F) = 10.1Hz, C), 148.88 (d, ^{1}J(C,F) = 245.7Hz, C), 150.70 (C), 155.14 (C), 155.81 (C), 159.81 (C), 165.24 (C), 166.76 (C), 169.90 (C), 172.72 (C), 174.11 (C) ppm. ^{19}F NMR (DMSO-d_6, 377 MHz): $\delta = -136.27$ ppm HRMS: $C_{39}H_{39}ClFN_6O_8S$ [M+H] calculated: 805.2217, found: 805.2217 HPLC: Purity: 98.8%

PROTAC ***SK3251*** is synthesized following the general protocol for PROTAC synthesis (HATU coupling). The product was obtained as an off-white solid (53 mg) in 62% yield after column chromatography (DCM/MeOH 0 -> 6%). ^{1}H NMR (DMSO-d_6, 400 MHz): $\delta = 1.57–1.93$ (m, 8H), 1.98–2.07 (m, 1H), 2.50–2.63 (m, 2H, overlap with solvent signal), 2.82–2.94 (m, 3H), 3.19 (q, $J = 5.7$Hz, 2H), 3.37 (t, $J = 6.0$Hz, 2H), 3.51 (m, 2H), 3.64 (m, 2H), 3.79 (m, 2H), 4.31 (m, 2H), 4.53 (br s, 1H), 5.08 (dd, J = 5.4; 12.8 Hz, 1H), 6.63 (d, $J = 7.3$Hz, 1H), 6.84 (d, $J = 8.2$Hz, 1H), 6.95 (d, $J = 3.6$Hz, 1H), 7.06–7.16 (m, 3H), 7.35 (d, $J = 3.6$Hz, 1H), 7.43 (d, $J = 7.2$Hz, 1H), 7.47–7.56 (m, 2H), 7.63 (t, $J = 5.4$Hz, 1H), 7.78 (dd, J = 7.4; 8.3Hz, 1H), 11.10 (m, 2H) ppm. ^{13}C NMR (DMSO-d_6, 100 MHz): $\delta = 21.99$ (CH2), 26.60 (CH2), 28.37 (CH2), 30.94 (CH2), 38.76 (CH2), 46.58 (C), 46.79 (CH2), 48.74 (CH), 68.68 (CH2), 68.86 (2x CH2), 69.59 (CH2), 70.12 (CH2), 74.32 (CH), 108.06 (CH), 110.65 (CH), 115.38 (CH), 116.15 (CH), 116.29 (C), 116.64 (CH), 119.93 (CH), 120.40 (d, ^{2}J(C,F) = 15.0Hz, C), 121.80 (CH), 124.90 (d, ^{3}J(C,F) = 4.9Hz, CH), 133.23 (C), 136.94 (CH), 137.37 (CH), 137.53 (CH), 146.20 (d, ^{2}J(C,F) = 10.1Hz, C), 148.88 (d, ^{1}J(C,F) = 245.7Hz, C), 150.70 (C), 155.13 (C), 155.78 (C), 159.81 (C), 165.26 (C), 166.78 (C), 169.93 (C), 172.76 (C), 174.10 (C) ppm. ^{19}F NMR (DMSO-d_6, 377 MHz): $\delta = -136.29$ ppm HRMS: $C_{41}H_{43}ClFN_6O_9S$ [M+H] calculated: 849.2479, found: 849.2480 HPLC: Purity: 98.8%

PROTAC ***SK2188*** is synthesized following the general protocol for PROTAC synthesis (HATU coupling). The product was obtained as an off-white solid (72 mg) in 81% yield after column chromatography (DCM/MeOH 0 -> 6%). ^{1}H NMR (DMSO-d_6, 400 MHz): $\delta = 1.58–1.93$ (m, 8H), 2.02 (m, 1H), 2.51–2.63 (m, 2H, overlap with solvent signal), 2.82–2.93 (m, 3H), 3.18 (m, 2H), 3.35 (m, 2H, overlap with H_2O signal), 3.44–3.55 (m, 6H), 3.60–3.66 (m, 2H), 3.78 (m, 2H), 4.31 (m, 2H), 4.54 (br s, 1H), 5.08 (dd, J = 5.4; 12.8 Hz, 1H), 6.63 (d, $J = 7.3$Hz, 1H), 6.86 (d, $J = 8.2$Hz, 1H), 6.95 (d, $J = 3.6$Hz, 1H), 7.05–7.18 (m, 3H), 7.35 (d, $J = 3.6$Hz, 1H), 7.44 (d, $J = 7.2$Hz, 1H), 7.48–7.57 (m, 2H), 7.62 (t, $J = 5.4$ Hz, 1H), 7.79 (dd, J = 7.4; 8.4Hz, 1H), 11.10 (m, 2H) ppm. ^{13}C NMR (DMSO-d_6, 100 MHz): $\delta = 22.00$ (CH2), 26.61 (CH2), 28.39 (CH2), 30.95 (CH2), 38.77 (CH2), 46.59 (C), 46.81 (CH2), 48.74 (CH), 68.69 (CH2), 68.83 (2x CH2), 69.53 (CH2), 69.76 (CH2), 69.84 (CH2), 70.17 (CH2), 74.35 (CH), 108.08 (CH), 110.66 (CH), 115.38 (CH), 116.17 (CH), 116.31 (C), 116.69 (CH), 119.97 (CH), 120.41 (d, ^{2}J(C,F) = 15.2Hz, C), 121.83 (CH), 124.92 (d, ^{3}J(C,F) = 4.8Hz, CH), 133.23 (C), 136.95 (CH), 137.38 (CH), 137.55 (CH), 146.20 (d, ^{2}J(C,F) = 10.1Hz, C), 148.90 (d, ^{1}J(C,F) = 245.8Hz, C), 150.72 (C), 155.15 (C), 155.81 (C), 159.83 (C), 165.26 (C), 166.80 (C), 169.93 (C), 172.78 (C), 174.12 (C) ppm. ^{19}F NMR (DMSO-d_6, 377 MHz): $\delta = -136.27$ ppm HRMS: $C_{43}H_{47}ClFN_6O_{10}S$ [M+H] calculated: 893.2742, found: 893.2738 HPLC: Purity: 97.3%

PROTAC ***SK2189*** is synthesized following the general protocol for PROTAC synthesis (HATU coupling). The product was obtained as an off-white solid (75 mg) in 80% yield after column chromatography (DCM/MeOH 0-> 6%). ^{1}H NMR (DMSO-d_6, 400 MHz): $\delta = 1.58–1.94$ (m, 8H), 1.98–2.07 (m, 1H), 2.50–2.63 (m, 2H, overlap with solvent signal), 2.82–2.93 (m, 3H), 3.18 (m, 2H), 3.35 (m, 2H, overlap with H_2O signal), 3.43–3.54 (m, 10H), 3.59–3.65 (m, 2H), 3.78 (m, 2H), 4.32 (m, 2H), 4.54 (br s, 1H), 5.08 (dd, J = 5.3; 12.8 Hz, 1H), 6.63 (d, $J = 7.3$Hz, 1H), 6.86 (d, $J = 8.2$Hz, 1H), 6.95 (d, $J = 3.6$Hz, 1H), 7.07–7.17 (m, 3H), 7.35 (d, $J = 3.6$Hz, 1H), 7.45 (d, $J = 7.2$Hz, 1H), 7.49–7.57 (m, 2H), 7.62 (t, $J = 5.5$Hz, 1H), 7.79 (dd, J = 7.4; 8.4Hz, 1H), 11.10 (m, 2H) ppm. ^{13}C NMR (DMSO-d_6, 100 MHz): $\delta = 22.00$ (CH2), 26.62 (CH2), 28.38 (CH2), 30.95 (CH2), 38.76 (CH2), 46.60 (C), 46.82 (CH2), 48.75 (CH), 68.68 (CH2), 68.84 (2x CH2), 69.52 (CH2), 69.73 (CH2), 69.78 (2x CH2), 69.82 (CH2), 70.15 (CH2), 74.37 (CH), 108.08 (CH), 110.66 (CH), 115.39 (CH), 116.17 (CH), 116.32 (C), 116.71 (CH), 120.01 (CH), 120.42 (d, ^{2}J(C,F) = 14.9Hz, C), 121.85 (CH), 124.93 (d, ^{3}J(C,F) = 4.9Hz, CH), 133.24 (C), 136.97 (CH), 137.38 (CH), 137.56 (CH), 146.21 (d, ^{2}J(C,F) = 10.0Hz, C), 148.91 (d, ^{1}J(C,F) = 245.9Hz, C), 150.73 (C), 155.15 (C), 155.83 (C), 159.83 (C), 165.26 (C), 166.81 (C), 169.93 (C), 172.78 (C), 174.12 (C) ppm. ^{19}F NMR (DMSO-d_6, 377 MHz): $\delta = -136.27$ ppm HRMS: $C_{45}H_{51}ClFN_6O_{11}S$ [M+H] calculated: 937.3004, found: 937.3004 HPLC: Purity: 97.9%

PROTAC ***SK3277*** is synthesized following the general protocol for PROTAC synthesis (HATU coupling). The product was obtained as an off-white solid (55 mg) in 68% yield after column chromatography (DCM/MeOH 0.5 -> 6%). ^{1}H NMR (DMSO-d_6, 400 MHz): $\delta = 1.58–1.93$ (m, 8H), 1.98–2.08 (m, 1H), 2.48–2.60 (m, 2H, overlap with solvent signal), 2.82–2.94 (m, 3H), 3.19–3.26 (m, 2H), 3.46 (t, $J = 6.0$ Hz, 2H), 3.72–3.79 (m, 2H), 4.25–4.32 (m, 2H), 4.49 (s, 1H), 5.11 (dd, J = 5.4; 12.8 Hz, 1H), 6.63 (d, $J = 7.3$Hz, 1H), 6.85 (d, $J = 8.2$Hz, 1H), 6.95 (d, $J = 3.6$Hz, 1H), 7.06–7.12 (m, 3H), 7.33 (dd, J = 2.3; 8.3 Hz, 1H), 7.35 (d, $J = 3.6$ Hz, 1H), 7.43 (d, $J = 2.2$Hz, 1H), 7.51 (t, $J = 8.0$ Hz, 1H), 7.66 (t, $J = 5.5$Hz, 1H), 7.80 (d, $J = 8.3$ Hz, 1H), 11.11 (s, 2H) ppm. ^{13}C NMR (DMSO-d_6, 100 MHz): $\delta = 22.1$ (CH2), 26.6 (CH2), 28.3 (CH2), 30.9 (CH2), 38.7 (CH2), 46.6 (C), 46.9 (CH2), 48.9 (CH), 68.3 (CH2), 68.4 (CH2), 69.0 (CH2), 74.3 (CH), 108.0 (CH), 108.8 (CH), 110.7 (CH), 116.1 (CH), 116.7 (CH), 120.4 (d, ^{2}J(C,F) = 14.9 Hz, C), 120.8 (CH), 121.9 (CH), 123.1 (C), 124.9 (d, ^{3}J(C,F) = 4.9 Hz, CH), 125.3 (CH), 133.9 (C), 137.4 (CH), 137.5 (CH), 146.2 (d, ^{2}J(C,F) = 10.1Hz, C), 148.9 (d, ^{1}J(C,F) = 245.8Hz, C), 150.7 (C), 155.1 (C), 159.8 (C), 163.9 (C), 166.76 (C), 166.83 (C), 169.9 (C), 172.8 (C), 174.2 (C) ppm. ^{19}F NMR (DMSO-d_6, 377 MHz): $\delta = -136.27$ ppm HRMS: $C_{39}H_{39}ClFN_6O_8S$ [M + H^+] calculated: 805.2217, found: 805.2222 HPLC: Purity: 98.6%

PROTAC ***SK3278*** is synthesized following the general protocol for PROTAC synthesis (HATU coupling). The product was obtained as an off-white solid (72 mg) in 85% yield after column chromatography (DCM/MeOH 0.5 -> 6%). ^{1}H NMR (DMSO-d_6, 400 MHz): $\delta = 1.58–1.94$ (m, 8H), 1.98–2.08 (m, 1H), 2.48–2.60 (m, 2H, overlap with solvent signal), 2.82–2.94 (m, 3H), 3.16–3.23 (m, 2H), 3.38 (t, $J = 6.1$ Hz, 2H), 3.49–3.55 (m, 2H), 3.56–3.61 (m, 2H), 3.75–3.80 (m, 2H), 4.25–4.32

(m, 2H), 4.53 (s, 1H), 5.11 (dd, J = 5.3; 12.8 Hz, 1H), 6.63 (d, *J* = 7.3Hz, 1H), 6.85 (d, *J* = 8.2Hz, 1H), 6.95 (d, *J* = 3.6Hz, 1H), 7.05–7.16 (m, 3H), 7.32 (dd, J = 2.3; 8.3 Hz, 1H), 7.35 (d, *J* = 3.5 Hz, 1H), 7.42 (d, *J* = 2.2 Hz, 1H), 7.53 (t, *J* = 7.8 Hz, 1H), 7.64 (t, *J* = 5.5Hz, 1H), 7.80 (d, *J* = 8.3 Hz, 1H), 11.11 (s, 2H) ppm. ^{13}C NMR (DMSO-d_6, 100 MHz): δ = 22.1 (CH2), 26.6 (CH2), 28.4 (CH2), 31.0 (CH2), 38.8 (CH2), 46.6 (C), 46.8 (CH2), 49.0 (CH), 68.4 (CH2), 68.6 (CH2), 68.8 (CH2), 69.5 (CH2), 69.9 (CH2), 74.3 (CH), 108.1 (CH), 108.8 (CH), 110.7 (CH), 116.2 (CH), 116.6 (CH), 120.4 (d, ^{2}J(C,F) = 14.9 Hz, C), 120.8 (CH), 121.8 (CH), 123.1 (C), 124.9 (d, ^{3}J(C,F) = 4.8 Hz, CH), 125.2 (CH), 133.9 (C), 137.4 (CH), 137.5 (CH), 146.2 (d, ^{2}J(C,F) = 10.0 Hz, C), 148.9 (d, ^{1}J(C,F) = 245.7Hz, C), 150.7 (C), 155.1 (C), 159.8 (C), 163.9 (C), 166.76 (C), 166.83 (C), 169.9 (C), 172.8 (C), 174.1 (C) ppm. ^{19}F NMR (DMSO-d_6, 377 MHz): δ = −136.27 ppm HRMS: $C_{41}H_{43}ClFN_6O_9S$ [M+H] calculated: 849.2479, found: 849.2479 HPLC: Purity: 98.2%

PROTAC ***SK3286*** is synthesized following the general protocol for PROTAC synthesis (HATU coupling). The product was obtained as an off-white solid (67 mg) in 75% yield after column chromatography (DCM/MeOH 0.5 -> 8%). ^{1}H NMR (DMSO-d_6, 400 MHz): δ = 1.58–1.94 (m, 8H), 1.99–2.08 (m, 1H), 2.48–2.63 (m, 2H, overlap with solvent signal), 2.82–2.94 (m, 3H), 3.14–3.22 (m, 2H), 3.36 (t, *J* = 6.0 Hz, 2H), 3.45–3.60 (m, 8H), 3.73–3.79 (m, 2H), 4.25–4.31 (m, 2H), 4.54 (s, 1H), 5.11 (dd, J = 5.4; 12.9 Hz, 1H), 6.63 (d, *J* = 7.3Hz, 1H), 6.86 (d, *J* = 8.2Hz, 1H), 6.95 (d, *J* = 3.6Hz, 1H), 7.05–7.17 (m, 3H), 7.31–7.37 (m, 2H), 7.43 (d, *J* = 2.2 Hz, 1H), 7.53 (t, *J* = 7.7 Hz, 1H), 7.62 (t, *J* = 5.5Hz, 1H), 7.80 (d, *J* = 8.3 Hz, 1H), 11.11 (s, 2H) ppm. ^{13}C NMR (DMSO-d_6, 100 MHz): δ = 22.1 (CH2), 26.6 (CH2), 28.4 (CH2), 30.9 (CH2), 38.8 (CH2), 46.6 (C), 46.8 (CH2), 49.0 (CH), 68.4 (CH2), 68.6 (CH2), 68.8 (CH2), 69.5 (CH2), 69.8 (2x CH2), 70.0 (CH2), 74.4 (CH), 108.1 (CH), 108.9 (CH), 110.7 (CH), 116.2 (CH), 116.7 (CH), 120.4 (d, ^{2}J(C,F) = 15.1 Hz, C), 120.8 (CH), 121.8 (CH), 123.1 (C), 124.9 (d, ^{3}J(C,F) = 4.7 Hz, CH), 125.3 (CH), 133.9 (C), 137.4 (CH), 137.5 (CH), 146.2 (d, ^{2}J(C,F) = 10.2 Hz, C), 148.9 (d, ^{1}J(C,F) = 245.9Hz, C), 150.7 (C), 155.1 (C), 159.8 (C), 163.9 (C), 166.78 (C), 166.84 (C), 169.9 (C), 172.8 (C), 174.1 (C) ppm. ^{19}F NMR (DMSO-d_6, 377 MHz): δ = −136.27 ppm HRMS: $C_{43}H_{47}ClFN_6O_{10}S$ [M+H] calculated: 893.2742, found: 893.2741 HPLC: Purity: 98.6%

PROTAC ***SK3287*** is synthesized following the general protocol for PROTAC synthesis (HATU coupling). The product was obtained as an off-white solid (83 mg) in 89% yield after column chromatography (DCM/MeOH 0.5 -> 8%). ^{1}H NMR (DMSO-d_6, 400 MHz): δ = 1.58–1.94 (m, 8H), 1.99–2.08 (m, 1H), 2.48–2.63 (m, 2H, overlap with solvent signal), 2.82–2.94 (m, 3H), 3.14–3.22 (m, 2H), 3.36 (t, *J* = 6.1 Hz, 2H), 3.45–3.54 (m, 10H), 3.55–3.60 (m, 2H), 3.73–3.79 (m, 2H), 4.25–4.31 (m, 2H), 4.54 (s, 1H), 5.11 (dd, J = 5.4; 12.9 Hz, 1H), 6.63 (d, *J* = 7.3Hz, 1H), 6.86 (d, *J* = 8.2Hz, 1H), 6.95 (d, *J* = 3.6Hz, 1H), 7.05–7.17 (m, 3H), 7.33–7.38 (m, 2H), 7.44 (d, *J* = 2.2 Hz, 1H), 7.54 (t, *J* = 7.9 Hz, 1H), 7.62 (t, *J* = 5.5Hz, 1H), 7.82 (d, *J* = 8.3 Hz, 1H), 11.11 (s, 2H) ppm. ^{13}C NMR (DMSO-d_6, 100 MHz): δ = 22.1 (CH2), 26.6 (CH2), 28.4 (CH2), 30.9 (CH2), 38.8 (CH2), 46.6 (C), 46.8 (CH2), 49.0 (CH), 68.4 (CH2), 68.6 (CH2), 68.8 (CH2), 69.5 (CH2), 69.7 (CH2), 69.77 (2x CH2), 69.79 (CH2), 69.9 (CH2), 74.4 (CH), 108.1 (CH), 108.9 (CH), 110.7 (CH), 116.2 (CH), 116.7 (CH), 120.4 (d, ^{2}J(C,F) = 15.2 Hz, C), 120.9 (CH), 121.8 (CH), 123.1 (C), 124.9 (d, ^{3}J(C,F) = 4.8 Hz, CH), 125.3 (CH), 133.9 (C), 137.4 (CH), 137.5 (CH), 146.2 (d, ^{2}J(C,F) = 10.1 Hz, C), 148.9 (d, ^{1}J(C,F) = 245.8Hz, C), 150.7 (C), 155.1 (C), 159.8 (C), 163.9 (C), 166.78 (C), 166.84 (C), 169.9 (C), 172.8 (C), 174.1 (C) ppm. HRMS: $C_{45}H_{51}ClFN_6O_{11}S$ [M+H] calculated: 937.3004, found: 937.3004 HPLC: Purity: 98.3%

Funding sources

The research of the manuscript was supported/funded by FWO grants 1S80521N (Simon Krols) and 11M1422N (Muhammad Rishfi), Villa Joep, Kom op tegen kanker and Stichting tegen kanker (C/2020/1469).

Declaration of competing interest

The authors declare that they have no known competing financial interests or personal relationships that could have appeared to influence the work reported in this paper.

Data availability

Data will be made available on request.

Acknowledgment

We would like to thank Izet Karalic for technical assistance and measuring HRMS spectra, Stijn Couwenbergh and Vicky Amo-Addae for assistance with the assays on the patient-derived organoids and the VIB-UGent proteomics core (Francis Impens, Simon Devos, Sara Dufour & Teresa Maria) for their expertise on shotgun proteomics.

Appendix A. Supplementary data

Supplementary data to this article can be found online at https://doi.org/10.1016/j.ejmech.2022.115033.

Abbreviations

AURKA	aurora Kinase A
CRBN	cereblon
CHK1	checkpoint kinase 1
HBD	hydrogen bound donor
NB	neuroblastoma
PEG	polyethylene glycol
PROTAC	proteolysis targeting chimera
POI	protein of interest
RPA32	replication protein A 32
SAR	structure activity relationship.

References

[1] J. Otte, C. Dyberg, A. Pepich, J.I. Johnsen, MYCN function in neuroblastoma development, Front. Oncol. 10 (2021), https://doi.org/10.3389/fonc.2020.624079.

[2] S.N. Gröbner, B.C. Worst, J. Weischenfeldt, I. Buchhalter, K. Kleinheinz, V. A. Rudneva, P.D. Johann, G.P. Balasubramanian, M. Segura-Wang, S. Brabetz, S. Bender, B. Hutter, D. Sturm, E. Pfaff, D. Hübschmann, G. Zipprich, M. Heinold, J. Eils, C. Lawerenz, S. Erkek, S. Lambo, S. Waszak, C. Blattmann, A. Borkhardt, M. Kuhlen, A. Eggert, S. Fulda, M. Gessler, J. Wegert, R. Kappler, D. Baumhoer, S. Burdach, R. Kirschner-Schwabe, U. Kontny, A.E. Kulozik, D. Lohmann, S. Hettmer, C. Eckert, S. Bielack, M. Nathrath, C. Niemeyer, G.H. Richter, J. Schulte, R. Siebert, F. Westermann, J.J. Molenaar, G. Vassal, H. Witt, M. Zapatka, B. Burkhardt, C.P. Kratz, O. Witt, C.M.V. Tilburg, C.M. Kramm, G. Fleischhack, U. Dirksen, S. Rutkowski, M. Frühwald, K. Von Hoff, S. Wolf, T. Klingebiel, E. Koscielniak, P. Landgraf, J. Koster, A.C. Resnick, J. Zhang, Y. Liu, X. Zhou, A. J. Waanders, D.A. Zwijnenburg, P. Raman, B. Brors, U.D. Weber, P.A. Northcott, K. W. Pajtler, M. Kool, R.M. Piro, J.O. Korbel, M. Schlesner, R. Eils, D.T.W. Jones, P. Lichter, L. Chavez, S.M. Pfister, The landscape of genomic alterations across childhood cancers, Nature 555 (2018) 321–327, https://doi.org/10.1038/nature25480.

[3] P. Depuydt, J. Koster, V. Boeva, T.D. Hocking, F. Speleman, G. Schleiermacher, K. De Preter, Meta-mining of copy number profiles of high-risk neuroblastoma tumors, Sci. Data 5 (2018), https://doi.org/10.1038/sdata.2018.240.

[4] A.J. Wolpaw, R. Bayliss, G. Büchel, C.V. Dang, M. Eilers, W. Clay Gustafson, G. H. Hansen, N. Jura, S. Knapp, M.A. Lemmon, D. Levens, J.M. Maris, R. Marmorstein, S.J. Metallo, J.R. Park, L.Z. Penn, M. Rape, M.F. Roussel, K. M. Shokat, W.P. Tansey, K.A. Verba, S.M. Vos, W.A. Weiss, E. Wolf, Y.P. Mossé, Drugging the "Undruggable" MYCN oncogenic transcription factor: overcoming previous obstacles to impact childhood cancers, Cancer Res. 81 (2021) 1627–1632, https://doi.org/10.1158/0008-5472.CAN-20-3108.

[5] Z. Liu, S.S. Chen, S. Clarke, V. Veschi, C.J. Thiele, Targeting MYCN in pediatric and adult cancers, Front. Oncol. 10 (2021), https://doi.org/10.3389/fonc.2020.623679.

[6] X. Shang, S.M. Burlingame, M.F. Okcu, N. Ge, H.v. Russell, R.A. Egler, R.D. David, S.A. Vasudevan, J. Yang, J.G. Nuchtern, Aurora A is a negative prognostic factor and a new therapeutic target in human neuroblastoma, Mol. Cancer Therapeut. 8 (2009) 2461–2469, https://doi.org/10.1158/1535-7163.MCT-08-0857.

[7] T. Marumoto, D. Zhang, H. Saya, Aurora-A - a guardian of poles, Nat. Rev. Cancer 5 (2005) 42–50, https://doi.org/10.1038/nrc1526.

[8] L. Macůrek, A. Lindqvist, D. Lim, M.A. Lampson, R. Klompmaker, R. Freire, C. Clouin, S.S. Taylor, M.B. Yaffe, R.H. Medema, Polo-like kinase-1 is activated by aurora A to promote checkpoint recovery, Nature 455 (2008) 119–123, https://doi.org/10.1038/nature07185.

[9] T. Otto, S. Horn, M. Brockmann, U. Eilers, L. Schüttrumpf, N. Popov, A.M. Kenney, J.H. Schulte, R. Beijersbergen, H. Christiansen, B. Berwanger, M. Eilers, Stabilization of N-myc is a critical function of aurora A in human neuroblastoma, Cancer Cell 15 (2009) 67–78, https://doi.org/10.1016/j.ccr.2008.12.005.

[10] A.K. Byrum, D. Carvajal-Maldonado, M.C. Mudge, D. Valle-Garcia, M.C. Majid, R. Patel, M.E. Sowa, S.P. Gygi, J. Wade Harper, Y. Shi, A. Vindigni, N. Mosammaparast, Mitotic regulators TPX2 and Aurora A protect DNA forks during replication stress by counteracting 53BP1 function, JCB (J. Cell Biol.) 218 (2019) 422–432, https://doi.org/10.1083/jcb.201803003.

[11] G. Büchel, A. Carstensen, K.Y. Mak, I. Roeschert, E. Leen, O. Sumara, J. Hofstetter, S. Herold, J. Kalb, A. Baluapuri, E. Poon, C. Kwok, L. Chesler, H.M. Maric, D. S. Rickman, E. Wolf, R. Bayliss, S. Walz, M. Eilers, Association with aurora-A controls N-MYC-Dependent promoter escape and pause release of RNA polymerase II during the cell cycle, Cell Rep. 21 (2017) 3483–3497, https://doi.org/10.1016/j.celrep.2017.11.090.

[12] J. de Wyn, M.W. Zimmerman, N. Weichert-leahey, C. Nunes, B.B. Cheung, B. J. Abraham, A. Beckers, P.J. Volders, B. Decaesteker, D.R. Carter, A.T. Look, K. de Preter, W. van Loocke, G.M. Marshall, A.D. Durbin, F. Speleman, K. Durinck, Meis2 is an adrenergic core regulatory transcription factor involved in early initiation of th-mycn-driven neuroblastoma formation, Cancers 13 (2021), https://doi.org/10.3390/cancers13194783.

[13] H. Beltran, C. Oromendia, D.C. Danila, B. Montgomery, C. Hoimes, R. Z. Szmulewitz, U. Vaishampayan, A.J. Armstrong, M. Stein, J. Pinski, J. M. Mosquera, V. Sailer, R. Bareja, A. Romanel, N. Gumpeni, A. Sboner, E. Dardenne, L. Puca, D. Prandi, M.A. Rubin, H.I. Scher, D.S. Rickman, F. Demichelis, D.M. Nanus, K.v. Ballman, S.T. Tagawa, A phase II trial of the aurora kinase a inhibitor alisertib for patients with castration-resistant and neuroendocrine prostate cancer: efficacy and biomarkers, Clin. Cancer Res. 25 (2019) 43–51, https://doi.org/10.1158/1078-0432.CCR-18-1912.

[14] M. Békés, D.R. Langley, C.M. Crews, PROTAC targeted protein degraders: the past is prologue, Nat. Rev. Drug Discov. 21 (2022) 181–200, https://doi.org/10.1038/s41573-021-00371-6.

[15] B. Adhikari, J. Bozilovic, M. Diebold, J.D. Schwarz, J. Hofstetter, M. Schröder, M. Wanior, A. Narain, M. Vogt, N. Dudvarski Stankovic, A. Baluapuri, L. Schönemann, L. Eing, P. Bhandare, B. Kuster, A. Schlosser, S. Heinzlmeir, C. Sotriffer, S. Knapp, E. Wolf, PROTAC-mediated degradation reveals a non-catalytic function of AURORA-A kinase, Nat. Chem. Biol. 16 (2020) 1179–1188, https://doi.org/10.1038/s41589-020-00652-y.

[16] R. Wang, C. Ascanelli, A. Abdelbaki, A. Fung, T. Rasmusson, I. Michaelides, K. Roberts, C. Lindon, Selective targeting of non-centrosomal AURKA functions through use of a targeted protein degradation tool, Commun Biol 4 (2021), https://doi.org/10.1038/s42003-021-02158-2.

[17] K.A. Donovan, F.M. Ferguson, J.W. Bushman, N.A. Eleuteri, D. Bhunia, S.S. Ryu, L. Tan, K. Shi, H. Yue, X. Liu, D. Dobrovolsky, B. Jiang, J. Wang, M. Hao, I. You, M. Teng, Y. Liang, J. Hatcher, Z. Li, T.D. Manz, B. Groendyke, W. Hu, Y. Nam, S. Sengupta, H. Cho, I. Shin, M.P. Agius, I.M. Ghobrial, M.W. Ma, J. Che, S. J. Buhrlage, T. Sim, N.S. Gray, E.S. Fischer, Mapping the degradable kinome provides a resource for expedited degrader development, Cell 183 (2020) 1714–1731, https://doi.org/10.1016/j.cell.2020.10.038, e10.

[18] J. Tang, R. Moorthy, Ö. Demir, Z.D. Baker, J.A. Naumann, K.F.M. Jones, M. J. Grillo, E.S. Haefner, K. Shi, M.J. Levy, H. Aihara, R.S. Harris, R.E. Amaro, N. M. Levinson, D.A. Harki, Targeting N-myc in neuroblastoma with selective aurora kinase A degraders, bioRxiv (2022), https://doi.org/10.1101/2022.04.09.487756.

[19] J. Bozilovic, L. Eing, B.-T. Berger, B. Adhikari, J. Weckesser, N.B. Berner, S. Wilhelm, B. Kuster, E. Wolf, S. Knapp, Novel, highly potent PROTACs targeting AURORA-A kinase, Current Research in Chemical Biology 2 (2022), 100032, https://doi.org/10.1016/j.crchbi.2022.100032.

[20] C.O. de Groot, J.E. Hsia, J.v. Anzola, A. Motamedi, M. Yoon, Y.L. Wong, D. Jenkins, H.J. Lee, M.B. Martinez, R.L. Davis, T.C. Gahman, A. Desai, A.K. Shiau, A cell biologist's field guide to aurora kinase inhibitors, Front. Oncol. 5 (2015), https://doi.org/10.3389/fonc.2015.00285.

[21] C. Cantrill, P. Chaturvedi, C. Rynn, J. Petrig Schaffland, I. Walter, M.B. Wittwer, Fundamental aspects of DMPK optimization of targeted protein degraders, Drug Discov. Today 25 (2020) 969–982, https://doi.org/10.1016/j.drudis.2020.03.012.

[22] S.D. Edmondson, B. Yang, C. Fallan, Proteolysis targeting chimeras (PROTACs)in 'beyond rule-of-five' chemical space: recent progress and future challenges, Bioorg. Med. Chem. Lett 29 (2019) 1555–1564, https://doi.org/10.1016/j.bmcl.2019.04.030.

[23] R.P. Nowak, S.L. Deangelo, D. Buckley, Z. He, K.A. Donovan, J. An, N. Safaee, M. P. Jedrychowski, C.M. Ponthier, M. Ishoey, T. Zhang, J.D. Mancias, N.S. Gray, J. E. Bradner, E.S. Fischer, Plasticity in binding confers selectivity in ligand-induced protein degradation article, Nat. Chem. Biol. 14 (2018) 706–714, https://doi.org/10.1038/s41589-018-0055-y.

[24] A. Zorba, C. Nguyen, Y. Xu, J. Starr, K. Borzilleri, J. Smith, H. Zhu, K.A. Farley, W. D. Ding, J. Schiemer, X. Feng, J.S. Chang, D.P. Uccello, J.A. Young, C.N. Garcia-Irrizary, L. Czabaniuk, B. Schuff, R. Oliver, J. Montgomery, M.M. Hayward, J. Coe, J. Chen, M. Niosi, S. Luthra, J.C. Shah, A. El-Kattan, X. Qiu, G.M. West, M.C. Noe, V. Shanmugasundaram, A.M. Gilbert, M.F. Brown, M.F. Calabrese, Delineating the role of cooperativity in the design of potent PROTACs for BTK, Proc. Natl. Acad. Sci. U. S. A. 115 (2018) E7285–E7292, https://doi.org/10.1073/pnas.1803662115.

[25] V. Zoppi, S.J. Hughes, C. Maniaci, A. Testa, T. Gmaschitz, C. Wieshofer, M. Koegl, K.M. Riching, D.L. Daniels, A. Spallarossa, A. Ciulli, Iterative design and optimization of initially inactive proteolysis targeting chimeras (PROTACs) identify VZ185 as a potent, fast, and selective von Hippel-lindau (VHL) based dual degrader probe of BRD9 and BRD7, J. Med. Chem. 62 (2019) 699–726, https://doi.org/10.1021/acs.jmedchem.8b01413.

[26] T. Bemis, J. la Clair, M. Burkart, Unraveling the role of linker design in proteolysis targeting chimeras, J. Med. Chem. 64 (2021) 8042–8052, https://doi.org/10.1021/acs.jmedchem.1c00482.

[27] N. Bai, S.A. Miller, G.v. Andrianov, M. Yates, P. Kirubakaran, J. Karanicolas, Rationalizing PROTAC-mediated ternary complex formation using rosetta, J. Chem. Inf. Model. 61 (2021) 1368–1382, https://doi.org/10.1021/acs.jcim.0c01451.

[28] D. Zaidman, J. Prilusky, N. London, ProsetTac: rosetta based modeling of PROTAC mediated ternary complexes, J. Chem. Inf. Model. 60 (2020) 4894–4903, https://doi.org/10.1021/acs.jcim.0c00589.

[29] T.M. Leissing, L.M. Luh, P.M. Cromm, Structure driven compound optimization in targeted protein degradation, Drug Discov. Today Technol. 37 (2020) 73–82, https://doi.org/10.1016/j.ddtec.2020.11.005.

[30] S.J. Hughes, A. Ciulli, Molecular recognition of ternary complexes: a new dimension in the structure-guided design of chemical degraders, Essays Biochem. 61 (2017) 505–516, https://doi.org/10.1042/EBC20170041.

[31] P. Pal, D. Thummuri, D. Lv, X. Liu, P. Zhang, W. Hu, S.K. Poddar, N. Hua, S. Khan, Y. Yuan, X. Zhang, D. Zhou, G. Zheng, Discovery of a novel BCL-XLPROTAC degrader with enhanced BCL-2 inhibition, J. Med. Chem. 64 (2021) 14230–14246, https://doi.org/10.1021/acs.jmedchem.1c00517.

[32] B.E. Smith, S.L. Wang, S. Jaime-Figueroa, A. Harbin, J. Wang, B.D. Hamman, C. M. Crews, Differential PROTAC substrate specificity dictated by orientation of recruited E3 ligase, Nat. Commun. 10 (2019), https://doi.org/10.1038/s41467-018-08027-7.

[33] X. Han, L. Zhao, W. Xiang, C. Qin, B. Miao, D. McEachern, Y. Wang, H. Metwally, L. Wang, A. Matvekas, B. Wen, D. Sun, S. Wang, Strategies toward discovery of potent and orally bioavailable proteolysis targeting chimera degraders of androgen receptor for the treatment of prostate cancer, J. Med. Chem. 64 (2021) 12831–12854, https://doi.org/10.1021/acs.jmedchem.1c00882.

[34] J. Zhang, J. Che, X. Luo, M. Wu, W. Kan, Y. Jin, H. Wang, A. Pang, C. Li, W. Huang, S. Zeng, W. Zhuang, Y. Wu, Y. Xu, Y. Zhou, J. Li, X. Dong, Structural feature analyzation strategies toward discovery of orally bioavailable PROTACs of bruton's tyrosine kinase for the treatment of lymphoma, J. Med. Chem. (2022), https://doi.org/10.1021/acs.jmedchem.2c00324.

[35] U. Nguyen, N. Squaglia, A. Boge, P.A. Fung, The Simple Western™: a gel-free, blot-free, hands-free Western blotting reinvention, Nat. Methods 8 (2011), https://doi.org/10.1038/nmeth.f.353 v–vi.

[36] Y. Yang, L. Ding, Q. Zhou, L. Fen, Y. Cao, J. Sun, X. Zhou, A. Liu, Silencing of AURKA augments the antitumor efficacy of the AURKA inhibitor MLN8237 on neuroblastoma cells, Cancer Cell Int. 20 (2020) 9, https://doi.org/10.1186/s12935-019-1072-y.

[37] Z. Kozicka, N.H. Thomä, Haven't got a glue: protein surface variation for the design of molecular glue degraders, Cell Chem Biol 28 (2021) 1032–1047, https://doi.org/10.1016/j.chembiol.2021.04.009.

[38] A. Pike, B. Williamson, S. Harlfinger, S. Martin, D.F. McGinnity, Optimising proteolysis-targeting chimeras (PROTACs) for oral drug delivery: a drug metabolism and pharmacokinetics perspective, Drug Discov. Today 25 (2020) 1793–1800, https://doi.org/10.1016/j.drudis.2020.07.013.

[39] L. Goracci, J. Desantis, A. Valeri, B. Castellani, M. Eleuteri, G. Cruciani, Understanding the metabolism of proteolysis targeting chimeras (PROTACs): the next step toward pharmaceutical applications, J. Med. Chem. 63 (2020) 11615–11638, https://doi.org/10.1021/acs.jmedchem.0c00793.

[40] Y. Iwasawa, T. Kato, N. Kwasnishi, K. Masutani, T. Mita, K. Nonoshita, M. Ohkubo, Novel aminopyridine derivatives having aurora A selective inhibitory action, Patent WO 2008/02678 A1, March 6, 2008, n.d.

[41] G.M. Burslem, P. Ottis, S. Jaime-Figueroa, A. Morgan, P.M. Cromm, M. Toure, C. M. Crews, Efficient synthesis of immunomodulatory drug analogues enables exploration of structure–degradation relationships, ChemMedChem 13 (2018) 1508–1512, https://doi.org/10.1002/cmdc.201800271.

[42] A. Bricelj, Y.L. Dora Ng, D. Ferber, R. Kuchta, S. Müller, M. Monschke, K. G. Wagner, J. Krönke, I. Sosič, M. Gütschow, C. Steinebach, Influence of linker attachment points on the stability and neosubstrate degradation of cereblon ligands, ACS Med. Chem. Lett. 12 (2021) 1733–1738, https://doi.org/10.1021/acsmedchemlett.1c00368.

[43] A. Bricelj, C. Steinebach, R. Kuchta, M. Gütschow, I. Sosič, E3 ligase ligands in successful PROTACs: an overview of syntheses and linker attachment points, Front. Chem. 9 (2021), https://doi.org/10.3389/fchem.2021.707317.

[44] A.A. Akuffo, A.Y. Alontaga, R. Metcalf, M.S. Beatty, A. Becker, J.M. McDaniel, R. S. Hesterberg, W.E. Goodheart, S. Gunawan, M. Ayaz, Y. Yang, M. Rezaul Karim, M.E. Orobello, K. Daniel, W. Guida, J.A. Yoder, A.M. Rajadhyaksha, E. Schönbrunn, H.R. Lawrence, N.J. Lawrence, P.K. Epling-Burnette, Ligand-mediated protein degradation reveals functional conservation among sequence variants of the CUL4-type E3 ligase substrate receptor cereblon, J. Biol. Chem. 293 (2018) 6187–6200, https://doi.org/10.1074/jbc.M117.816868.

[45] C. Nunes, J. Anckaert, F. de Vloed, J. de Wyn, K. Durinck, J. Vandesompele, F. Speleman, V. Vermeirssen, HTSplotter: an end-to-end data processing, analysis and visualisation tool for chemical and genetic in vitro perturbation screening | Enhanced Reader, bioRxiv (2022).

[46] C. Chiva, R. Olivella, E. Borràs, G. Espadas, O. Pastor, A. Solé, E. Sabidó, QCloud: a cloud-based quality control system for mass spectrometry-based proteomics laboratories, PLoS One 13 (2018), e0189209, https://doi.org/10.1371/journal.pone.0189209.
[47] V. Demichev, C.B. Messner, S.I. Vernardis, K.S. Lilley, M. Ralser, DIA-NN: neural networks and interference correction enable deep proteome coverage in high throughput, Nat. Methods 17 (2020) 41–44, https://doi.org/10.1038/s41592-019-0638-x.
[48] X. Zhang, A.H. Smits, G.B. van Tilburg, H. Ovaa, W. Huber, M. Vermeulen, Proteome-wide identification of ubiquitin interactions using UbIA-MS, Nat. Protoc. 13 (2018) 530–550, https://doi.org/10.1038/nprot.2017.147.
[49] M.E. Ritchie, B. Phipson, D. Wu, Y. Hu, C.W. Law, W. Shi, G.K. Smyth, Limma powers differential expression analyses for RNA-sequencing and microarray studies, Nucleic Acids Res. 43 (2015), https://doi.org/10.1093/nar/gkv007 e47–e47.